NACA TN No. 1499

NATIONAL ADVISORY COMMITTEE FOR AERONAUTICS

TECHNICAL NOTE

No. 1499

THE INWARD BULGE TYPE BUCKLING OF MONOCOQUE CYLINDERS IV - EXPERIMENTAL INVESTIGATION OF CYLINDERS SUBJECTED TO PURE BENDING

By N. J. Hoff, Bruno A. Boley, and S. V. Nardo

Polytechnic Institute of Brooklyn

Washington
September 1948

NATIONAL ADVISORY COMMITTEE FOR AERONAUTICS

TECHNICAL NOTE NO. 1499

THE INWARD BULGE TYPE BUCKLING OF MONOCOQUE CYLINDERS IV - EXPERIMENTAL INVESTIGATION OF CYLINDERS SUBJECTED TO PURE BENDING

By N. J. Hoff, Bruno A. Boley, and S. V. Nardo

SUMMARY

Eighteen 24S-T Alclad cylinders of 20-inch diameter, with skin thickness varying between 0.012 inch and 0.025 inch and length varying between 40.5 inches and 64 inches, were tested in pure bending. They were reinforced with either 16 or 28 stringers and either 5 or 6 rings.

One of the purposes of the investigation was to establish the critical value of the parameter Λ, that is, a value above which failure would occur by general instability and below which panel instability would take place. This value was found to be between 20 and 40 for cylinders with 16 stringers and between 16 and 74 for cylinders with 28 stringers.

The results of the experiments check the theory given in the paper entitled "General Instability of Monocoque Cylinders" by N. J. Hoff (Jour. Aero. Sci., vol. 10, no. 4, April 1943, pp. 105 - 114, 130) and are presented in graphical form for the convenience of the designer. Calculations were also carried out which show that the fuselages of four modern transport airplanes have values of Λ close to the transition region. This is desirable since then the fuselages are of equal strength from the standpoints of panel and general instability failure.

INTRODUCTION

The constant demand for a more efficient design of the semimonocoque type of construction has brought to the foreground the problem of general instability. Accordingly, both theoretical and experimental research concerned with this type of failure has been conducted at first at the Guggenheim Aeronautical Laboratory of the California Institute of Technology (references 1 to 5) and more recently at the Polytechnic Institute of Brooklyn Aeronautical Laboratories (references 6 to 8).

The present report describes pure bending tests carried out at PIBAL with 18 reinforced monocoque cylinders. Suggestions are given both as to the determination of the type of structure which will be likely to fail by general instability and as to a method of buckling load calculation which is convenient for design purposes and is verified by the available empirical data.

General instability is defined as the simultaneous buckling of the longitudinal and circumferential reinforcing elements of a monocoque cylinder, as well as the sheet covering attached to them. In monocoques subjected to pure bending, general instability is usually of the inward bulge type, so-called because it is characterized by the appearance of an inward bulge symmetric to the most highly compressed stringer and extending over a number of rings. The distorted shape of the stringers approximately resembles a sine curve, the half wave length of which is longer than the distance between adjacent rings. If the dimensions of the rings, however, are sufficiently increased relative to the size of the stringers, the wave length decreases and becomes equal to the ring spacing. Inasmuch as the distortions are then confined to stringers and sheet covering between adjacent rings only, this type of failure is denoted as panel instability.

It is shown in reference 6 that a critical value exists for the parameter Λ defined in equation (4) which is the dividing point between general and panel instability. It is indicated in that reference that this critical value lies between 10 and 200. Because of the lack of sufficient experimental data in this region, two series of specimens with a different number of stringers were designed and tested in order to supply the desired information.

Reference 9 suggests a procedure for the evaluation of the critical stress in general instability, the reliability of which depends on the knowledge of the value of the parameter n. A graph giving values of this parameter based on the GALCIT tests was shown in that reference; it is presented in this report as modified by the results of a third series of cylinders included in the present experimental investigation as well as by the results of reference 7. The original graph has also been revised to account for the effect of the variation of the modulus above the proportional limit.

The authors are indebted to Mr. Bernard Levine for his contribution to the design and testing of the experimental specimens and to the evaluation of the results. The cooperation of Canadair, Limited, Pan American Airways System, Republic Aviation Corporation, and Boeing Aircraft Company in supplying data concerning some of their airplanes is gratefully acknowledged.

This work was conducted at the Polytechnic Institute of Brooklyn under the sponsorship and with the financial assistance of the National Advisory Committee for Aeronautics.

SYMBOLS

A_{str}	area of stringer plus effective width of sheet
d	stringer spacing measured along circumference
E	Young's modulus
E_r	Young's modulus for ring
E_{str}	Young's modulus for stringer
F_{cy}	compressive yield point
I_r	moment of inertia of ring plus effective width of sheet
I_{str_r}	stringer moment of inertia for radial bending
I_{str_t}	stringer moment of inertia for tangential bending
k	dimensionless coefficient used in calculating buckling stress of flat sheet
L_1	distance between adjacent rings
n	parameter required in calculation of buckling strain
r	radius of cylinder
t	thickness of sheet covering
2w	effective width of flat panel
2w'	effective width of curved panel
ϵ_{cr}	critical strain in most highly compressed stringer
ϵ_{curved}	buckling strain of nonreinforced circular cylinder under uniform axial compression
ϵ_{flat}	critical strain in flat panel under uniform axial compression
ϵ_{str}	strain in stringer
$\Lambda = (r^4/L_1{}^3 d)(E_{str}I_{str}/E_r I_r)$	
μ	Poisson's ratio

TEST SPECIMENS, RIG, AND PROCEDURE

Twelve cylinders with 16 stringers and six with 28 stringers were tested – in all 18 cylinders – which were numbered consecutively from 44 to 61. A drawing of a typical test specimen is presented in figure 1, and detailed characteristics of each cylinder are contained in table I.

All cylinders had a 20-inch diameter and a length varying between 40.5 inches and 64 inches. The sheet was 24S-T Alclad aluminum alloy 0.012 inch thick in all specimens except cylinder 53 (thickness t = 0.025 in.; 24S-T) and cylinders 54 and 55 (t = 0.020 in.; 24S-T). The longitudinal reinforcement consisted of either 16 or 28 stringers equally spaced along the circumference on the inside of the sheet covering. The stringers were of 24S-T aluminum alloy and of either square or rectangular cross section in all test specimens. The circumferential reinforcement was provided by either five or six 24S-T aluminum-alloy rings placed on the outside of the sheet. Their cross section was either square or rectangular, except in cylinder 57, in which the rings were hexagonal, 1/4 inch across flats. The ring spacing, constant in any one cylinder, varied between specimens from 5.79 inches to 9.00 inches.

The rings and stringers were attached to the skin by means of $\frac{1}{8}$-inch A17S-T aluminum-alloy round-head rivets. The rivet spacing was 0.643 inch on the stringers and approximately 1 inch on the rings. The rings and stringers were fastened to each other at their intersection by $\frac{1}{8}$-inch steel machine screws, except in cylinder 60, in which the diameter of the screws was 3/32 inch.

The test rig and the attachment of the cylinders to it are very much the same as those used in the tests described in reference 10. Differences worth mentioning are a heavy stiffening grid of steel channels added to the end stand and a lever arrangement, operated by a mechanical jack, which permitted the application of higher loads than the previous interlinked frames system.

The load was measured by means of a pair of Baldwin-Southwark SR-4 type A-1 electric strain gages cemented to opposite sides of a calibrated load link. The strains were measured in alternate stringers in the ring fields next to the two end fields of each cylinder by pairs of SR-4 strain gages. Type A-11 strain gages were used in cylinder 50 and cylinders 56 to 61; in all the other specimens type A-1 gages were employed. The strain measurements with gages attached to the stringers were made with the aid of an SR-4 portable electronic strain indicator; readings on all other gages were obtained with an SR-4 control box. Switching was done by two Shallcross multiple switching units and by the tapered brass socket and plug arrangement used in the tests of reference 7. From five to eight load

increments of approximately 750 pounds to 1000 pounds were applied to each test specimen. At each stage of loading readings were taken and checked on all the strain gages.

As in the previous tests, the weight of the loading head and end ring was balanced by weights suspended on a cable passing over two sheaves. As was discussed in reference 11, in order to eliminate the application to the cylinders of an undesirable shear force, it was necessary to check at each stage of loading that the force in the cable would not vary. This was done by means of a calibrated load link inserted between the cable and the loading head. About 1 to 3 minutes were required to complete the change from one load to the next. Approximately 1/2 hour was necessary to obtain a complete set of readings and check readings at one stage of loading. A complete test to failure took from 4 to 8 hours and was always completed within 1 day. The accuracy of the strain measurements is believed to be better than a strain of $\pm 10 \times 10^{-6}$. The applied load was measured with an error of less than ± 50 pounds.

PRESENTATION OF TEST RESULTS

The strains measured in the stringers in the ring fields next to each end field were plotted for each specimen against the distance of the stringer from the horizontal diameter of the cylinder. These strain diagrams are shown for one band of each cylinder in figures 2 to 19. It was decided to present drawings corresponding to only one band of each cylinder since no material differences were found in any case between the two bands. Curves are given in these diagrams for four approximately evenly spaced stages of loading, the highest of which corresponds to an applied bending moment never lower than 60 percent but usually above 80 percent of the buckling moment. It may be observed from these curves that the strain distribution is linear in good approximation in all cylinders for loads smaller than one-half the buckling load. Deviations from linearity appear especially on the compression side of the cylinder when buckling of the sheet becomes pronounced and when the critical bending moment is approached. The strains measured at points symmetrical with respect to either of the two vertical planes of symmetry showed good agreement, except for the highest stages of loading.

A check on the accuracy of the measurements was obtained by calculating from the strain readings the values of the total bending moment and axial force in the two cross sections of each cylinder and by comparing these results with the externally applied loads. This check was carried out for a low applied bending moment and for a load corresponding approximately to one-half the maximum moment. The results for the two bands of each cylinder are collected in table II. This calculation required a knowledge of the effective width $2w'$ of sheet acting with each stringer when the strain was higher than the buckling strain of the skin. It was obtained from the following formulas:

$$\left.\begin{aligned} 2w' &= 2w + (\epsilon_{curved}/\epsilon_{str})(d - 2w) \\ 2w &= \left[\epsilon_{flat}/(\epsilon_{str} - \epsilon_{curved})\right]^{1/3} d \end{aligned}\right\} \quad (1)$$

where ϵ_{str} is the strain in the stringer and d is the stringer spacing measured along the circumference. These formulas were obtained from reference 12.

The buckling strain of the flat panel ϵ_{flat} was determined from the formula

$$\epsilon_{flat} = k \frac{\pi^2}{12(1 - \mu^2)} (t/d)^2 \quad (2)$$

where t is the thickness of the sheet, μ is Poisson's ratio, and k is a dimensionless coefficient depending on the length-to-width ratio of the panel and upon the edge conditions. The values of k for cylinders with 16 stringers were taken as 4, 4, and 5 when the sheet thickness was 0.025 inch, 0.020 inch, and 0.012 inch, respectively. For cylinders with 28 stringers the value of k was assumed to be 5.5. The value of k was varied with the thickness of the sheet because of the different amount of end restraint likely to be provided by the stringers in each case. The buckling strain ϵ_{curved} of the cylindrical sheet was evaluated from Donnell's formula:

$$\epsilon_{curved} = 0.6(t/r) \frac{1 - (1.7 \times 10^{-7})(r/t)^2}{1 + 0.004(E/F_{cy})} \quad (3)$$

where r is the radius of the cylinder and F_{cy} the compressive yield point of the material.

Inspection of the values of table II shows that reasonably good agreement was obtained between the calculated and measured values of force and moment at both loads given. The deviation in the bending moments is 10 percent or less of the measured load in all cases, except in cylinder 52 in which the discrepancy is as high as 20 percent and in the first load of cylinder 46, which shows a 15-percent variation. The calculated unbalanced axial force is generally considerably smaller than ±10 percent of the total tensile force in the cross section, with the exception of cylinder 58, in which the deviation is 24.7 percent in one of the bands.

Curves showing the variation with applied bending moment of the strain in the most highly compressed stringer were plotted for each cylinder. As no appreciable differences were exhibited by any of these graphs, they are shown only for three representative cylinders in figures 20, 21, and 22. In each figure curves are presented for each of the two bands. Except at very high loads, the two bands gave almost the same results. All curves were approximately straight lines at low loads, but the slope changed when buckling of the sheet covering decreased the effective area. The deviations became pronounced in many cases when the load approached the maximum moment. The maximum strain sustained by each cylinder at buckling was determined from these diagrams by extrapolating the average of the values obtained with each band. This extrapolated value was needed in connection with figures 23 and 24. Data pertaining to the failure of the cylinders are contained in table III.

The deflected shape of the specimens at failure may be seen from the photographs (figs. 25 to 40). No photographs were taken of cylinders 44 and 45. Variations of the distortions corresponding to panel or general instability are discussed in the next section. Table IV shows that the cylinders are able to support a large percentage of the buckling moment even after the instability bulge has formed. After each cylinder had collapsed, the load was not removed for at least 12 hours. The load was then taken off and increased again to the maximum possible value. This was on the average 91.5 percent of the original buckling moment. The lowest values were 79 percent for cylinder 47 and about 60 percent for cylinder 61.

THE CRITICAL VALUE OF Λ

The dimensionless parameter Λ is defined in reference 9 as

$$\Lambda = (r^4/L_1{}^3d)(E_{str}I_{str}/E_rI_r) \tag{4}$$

where

$$I_{str} = I_{str_r} + (5/8)(1/n^2)\, I_{str_t} \tag{4a}$$

In these equations I_r is the moment of inertia of the ring cross section; I_{str_r} and I_{str_t} are the moments of inertia of the stringer cross section for radial and tangential bending, respectively. The effective width of sheet should be included in the calculations of

the moments of inertia. In this report the width of sheet acting with the rings was taken equal to the width of the ring, and that acting with the stringers was calculated from equation (1). The parameter n appearing in equation (4a) may be taken from figure 24 of the present report, which is a modification of figure 10 of reference 9. If no better value is available, n may be taken equal to 3. A discussion of this parameter appears in the next section.

According to a discussion in reference 6, a monocoque cylinder always fails in general instability if the value of Λ corresponding to it is higher than approximately 200 and always fails in panel instability if Λ is lower than 10. In the region between 10 and 200 either type of failure may occur. As little experimental data existed covering this region, two series of specimens were tested with the aim of narrowing down the uncertain zone. The value of Λ was changed between cylinders of each series merely by changing the size of the rings.

The first series includes cylinders 44 to 49, each of which had 16 stringers. It may be seen from table III and from the photographs (figs. 25 to 28) that all cylinders in this series with a value of Λ equal to or larger than 38.5 failed in general instability, whereas the cylinder with Λ equal to 19.5 failed in panel instability. The failure of the specimen with a value of Λ of 30 started with a panel-instability pattern, which changed over suddenly at buckling to a general-instability type. It may be therefore concluded that for cylinders similar to those in this series failure will occur by panel instability if $\Lambda < 20$, failure will occur by general instability if $\Lambda > 40$, and either type may occur if $20 < \Lambda < 40$.

The second series is formed by cylinders 56 to 61, each of which was reinforced with 28 stringers. The results obtained with cylinders 56 and 57, however, should be used with caution. In cylinder 56 one of the bolts connecting a ring and a stringer at their intersection failed during buckling. For this reason cylinder 60 was built identical with cylinder 56, except that $\frac{5}{32}$-inch bolts were used to replace the previous $\frac{1}{8}$-inch size. In cylinder 57, which had $\frac{1}{4}$-inch hexagonal rings, collapse occurred by failure of one of the rings. No duplicate of this specimen was built. From table III and the photographs (figs. 37 to 40) the conclusions may be drawn that for $\Lambda < 16$ failure will occur by panel instability, for $16 < \Lambda < 74$ either type may occur, and for $\Lambda > 74$ failure will occur by general instability. These results are valid for specimens similar to those tested in this series.

The value of Λ was calculated for the fuselages of four modern transport airplanes, designated as models A, B, C, and D. The following values of Λ were obtained:

Model	Λ
A	66
B	72
C	15
D, upper section (r = 66 in.)	29
D, lower section (r = 57 in.)	12

From these results, it may be concluded that models A, B, and D, upper section, are likely to fail by general instability, whereas models C and D, lower section, would probably fail by panel instability. However, all the five values of Λ are either in or so close to the limits of the transition zone that the type of failure cannot be predicted with any degree of certainty. It may be mentioned that it is desirable to design fuselages so that they fall in the transition zone, since then they are equally strong from the standpoints of panel and general instability. Earlier airplanes had much lower values of Λ, as may be seen from reference 6, where Λ was calculated for a number of these transports. The values obtained ranged from 0.1308 to 3.844, except for one model for which Λ was 71.38. The rings of all these earlier types of airplane were unnecessarily heavy. They would prevent general instability up to loads which could never be reached because of the much lower critical loads in panel instability.

The types of failure predicted will occur provided that the fuselage does not fail at smaller loads for reasons not investigated here. For example, failure may be caused by a break through stringers and skin on the tension side or by collapse of a stringer due to beam-column action if a shear force is present which causes a tension diagonal field to develop.

In the calculation of Λ, values were used for the spacing and size of the various members of the fuselages which correspond to reasonable averages of the actual dimensions. In the fuselage of model B, however, the variation in the sizes was large enough to warrant a revision of the development of the theory on the basis of a variable moment of inertia of the stringers. A good approximation to the correct value of Λ may be usually obtained from the dimensions of the fuselage in the neighborhood of the most highly compressed stringers.

THE PARAMETER n

It was shown in reference 9 that the most highly compressed stringer in a monocoque cylinder subjected to pure bending would sustain at the moment of buckling by general instability a strain which may be calculated by the following equation:

$$\epsilon_{cr} = n^2\pi^2 I_{str}/(L_1{}^2 \Lambda^{1/2} A_{str}) \qquad (5)$$

where A_{str} is the area of a stringer plus effective width of sheet, I_{str} may be calculated from formula (4a), and L_1 is the ring spacing. After substitution in equation (5) of the value of Λ from equation (4), the strain may be written as

$$\epsilon_{cr} = \frac{n^2\pi^2}{r^2 A_{str}} \sqrt{\frac{d}{L_1} \frac{E_r}{E_{str}} I_{str} I_r} \qquad (6)$$

In reference 9 it is shown that the value of n depends on the dimensionless parameters r/d and $\epsilon_{cr}/\epsilon_{cr_{sh}}$, the latter of which may be represented approximately by $\epsilon_{cr} r/t$. Curves presented in figure 10 of that reference on the basis of the GALCIT tests show that this fact was substantiated by experiment. The dashed lines of figure 23 of the present report are identical with those of figure 10 of reference 9.

The values of n for cylinders 50 to 55, 59, and 61 were obtained from equation (6) in which the experimental extrapolated values of ϵ_{cr} had been substituted. These results are plotted as crosses in figure 23, together with the values of n similarly obtained for the cylinders of reference 7. The values of n given for the GALCIT cylinders in figure 10 of reference 9 are based on the assumption that Hooke's law holds. As, however, several cylinders failed under a strain higher than the proportional limit, the values of n were recalculated on the basis of a reduced modulus of elasticity. The tangent-modulus values of 24S-T aluminum alloy required for these calculations were taken from reference 13. It may be observed that the agreement between the points and the curves may be considerably improved by modifying the original lines in the manner indicated by the solid lines in figure 23.

It might be noted that some of the specimens of reference 2 were used in redrawing the curves in spite of the fact that a slight amount of compression was applied to them in addition to the bending moment.

The compressive force, however, was comparatively small and caused in the worst case a strain of 20.3 percent of the maximum strain in the cylinder. The inclusion of these points in figure 23 is warranted by the investigations of references 6 and 7.

The curves of figure 24 are identical with the solid lines of figure 23 and should be considered as the final result. When these curves are used to predict the buckling load of a cylinder the results may be calculated by a step-by-step approximations procedure. First, n may be assumed to be 3 and ϵ_{cr} calculated from equation (6). With this value of the critical strain a new value of n can be read from the curves of figure 24. The procedure must be continued until the assumed and calculated values of n are close enough for practical purposes. It should not be forgotten that I_{str} changes with n, as may be seen from equation (4a), and the effective width of the sheet changes with ϵ. The step-by-step procedure is shown in detail in reference 9.

CONCLUSIONS

On the basis of two series, each consisting of six cylinders tested at PIBAL, and the theoretical and experimental work reported in NACA TN's Nos. 938, 939, and 968, the likelihood of failure by panel or general instability may be decided from the following table:

r/d	General instability zone	Transition zone	Panel instability zone
2.54	$\Lambda > 40$	$20 < \Lambda < 40$	$\Lambda < 20$
4.46	$\Lambda > 74$	$16 < \Lambda < 74$	$\Lambda < 16$

In this table

$$\Lambda = (r^4/L_1{}^3d)(E_{str}I_{str}/E_rI_r)$$

Moreover

$$I_{str} = I_{str_r} + (5/8)(1/n^2)\, I_{str_t}$$

where

r	radius of cylinder
d	stringer spacing measured along circumference
L_1	distance between adjacent rings
E_{str}	Young's modulus for stringer
E_r	Young's modulus for ring
I_r	moment of inertia of ring plus effective width of sheet
n	parameter required in calculations of buckling strain
I_{str_r}	stringer moment of inertia for radial bending
I_{str_t}	stringer moment of inertia for tangential bending

In the transition zone either type of instability may occur.

The value of the failing strain ϵ_{cr} in general instability in the most highly compressed stringer in a monocoque cylinder subjected to pure bending may be calculated from the formula

$$\epsilon_{cr} = n^2\pi^2 I_{str}/(L_1{}^2\Lambda^{1/2}A_{str})$$

where A_{str} is the area of the stringer plus the effective width of the sheet. It may be seen from a plot of r/d against $\epsilon_{cr}\frac{r}{t}$ (where t is the thickness of sheet covering) that the value of n depends on the critical strain. A trial-and-error procedure is therefore necessary in order to evaluate the strain ϵ_{cr} from the foregoing equation.

Some caution should be exercised in using these recommendations since they are based on model tests and theory and no full-scale tests have yet been carried out to substantiate them.

Polytechnic Institute of Brooklyn
Brooklyn, N. Y., February 4, 1947

REFERENCES

1. GALCIT: Some Investigations of the General Instability of Stiffened Metal Cylinders. I – Review of Theory and Bibliography. NACA TN No. 905, 1943.

2. GALCIT: Some Investigations of the General Instability of Stiffened Metal Cylinders. II – Preliminary Tests of Wire-Braced Specimens and Theoretical Studies. NACA TN No. 906, 1943.

3. GALCIT: Some Investigations of the General Instability of Stiffened Metal Cylinders. III – Continuation of Tests of Wire-Braced Specimens and Preliminary Tests of Sheet-Covered Specimens. NACA TN No. 907, 1943.

4. GALCIT: Some Investigations of the General Instability of Stiffened Metal Cylinders. IV – Continuation of Tests of Sheet-Covered Specimens and Studies of the Buckling Phenomena of Unstiffened Circular Cylinders. NACA TN No. 908, 1943.

5. GALCIT: Some Investigations of the General Instability of Stiffened Metal Cylinders. V – Stiffened Metal Cylinders Subjected to Pure Bending. NACA TN No. 909, 1943.

6. Hoff, N. J., and Klein, Bertram: The Inward Bulge Type Buckling of Monocoque Cylinders. I – Calculation of the Effect upon the Buckling Stress of a Compressive Force, A Nonlinear Direct Stress Distribution, and a Shear Force. NACA TN No. 938, 1944.

7. Hoff, N. J., Fuchs, S. J., and Cirillo, Adam J.: The Inward Bulge Type Buckling of Monocoque Cylinders. II – Experimental Investigation of the Buckling in Combined Bending and Compression. NACA TN No. 939, 1944.

8. Hoff, N. J., and Klein, Bertram: The Inward Bulge Type Buckling of Monocoque Cylinders. III – Revised Theory Which Considers the Shear Strain Energy. NACA TN No. 968, 1945.

9. Hoff, N. J.: General Instability of Monocoque Cylinders. Jour. Aero. Sci., vol. 10, no. 4, April 1943, pp. 105–114, 130.

10. Hoff, N. J., and Boley, Bruno A.: Stresses in and General Instability of Monocoque Cylinders with Cutouts. I – Experimental Investigation of Cylinders with a Symmetric Cutout Subjected to Pure Bending. NACA TN No. 1013, 1946.

11. Hoff, N. J., Boley, Bruno A., and Viggiano, Louis R.: Stresses in and General Instability of Monocoque Cylinders with Cutouts. IV – Pure Bending Tests of Cylinders with Side Cutout. NACA TN No. 1264, 1948.

12. Ebner, H.: The Strength of Shell Bodies – Theory and Practice. NACA TM No. 838, 1937.

13. Templin, R. L., Hartmann, E. C., and Paul, D. A.: Typical Tensile and Compressive Stress-Strain Curves for Aluminum Alloy 24S-T, Alclad 24S-T, 24S-RT, and Alclad 24S-RT Products. Tech. Paper No. 6, Aluminum Research Labs., Aluminum Co. of Am., 1942.

TABLE I – CYLINDER CHARACTERISTICS

[Diameter, 20 in. for all cylinders; rivet spacing along stringers, 0.643 in., along rings, 1 in. approximately. $\frac{1}{8}$-inch machine screws for fastening rings and stringers at their intersections]

Cylinder	Stringer size (in. × in.)	Number of stringers	Ring size (in. × in.)	Number of rings	Ring spacing (in.)	Length of cylinder (in.)	Sheet thickness (in.)	Λ
44	3/8 × 3/8	16	3/8 × 1/8	5	7.07	48	0.012	241
45	-----do----	--do--	1/2 × 1/8	--do--	--do--	48	--do--	174
46	-----do----	--do--	1/4 × 1/4	--do--	--do--	48	--do--	38
47	-----do----	--do---	3/4 × 3/16	--do--	--do--	48	--do--	30
48	-----do----	--do--	1 × 1/8	--do--	--do--	48	--do--	76
49	-----do----	--do--	1/4 × 1/2	--do--	--do--	48	--do--	19
50	5/16 × 5/16	--do--	1/8 × 1/2	6	5.79	46	--do--	180
51	3/8 × 3/8	--do--	----do----	--do--	6.43	$50\frac{1}{2}$	--do--	228
52	1/2 × 1/2	--do--	----do----	--do--	5.79	46	--do--	830
53	-----do----	--do--	1/8 × 3/8	5	9.00	$59\frac{1}{2}$	.025	344
54	3/8 × 3/4	--do--	1/8 × 3/8	6	6.43	$50\frac{1}{2}$	.020	612
55	-----do----	--do--	1/8 × 1/2	--do--	5.79	46	--do--	725
56	1/4 × 1/2	28	3/16 × 1/2	5	9.00	$59\frac{1}{2}$	.012	16
57	-----do-----	--do--	1/4 hexagonal	--do--	--do--	62	--do--	21
58	-----do----	--do--	1/8 × 3/4	--do--	--do--	62	--do--	35
59	-----do----	--do--	1/8 × 1/2	--do--	--do--	62	--do--	54
60	-----do----	--do--	3/16 × 1/2	--do--	--do--	62	--do--	16
61	-----do----	--do--	1/8 × 3/8	--do--	--do--	62	--do--	74

TABLE II – FORCE AND MOMENT EQUILIBRIUM

[Moments not corrected for tare weight of apparatus]

	Low load		High load		Low load		High load		Low load		High load	
	Moment (lb–in.)	Force (lb)	Moment (lb–in.)	Force (lb)	Moment (lb–in.)	Force (lb)	Moment (lb–in.)	Force (lb)	Moment (lb–in.)	Force (lb)	Moment (lb–in.)	Force (lb)
	Cylinder 44				Cylinder 45				Cylinder 46			
Applied	36,800	0	73,000	0	35,700	0	179,200	0	54,600	0	220,900	0
Band B	34,700	23	68,200	42	32,000	–70	164,400	41	46,400	–183	205,800	–289
Band E	35,500	42	69,900	94	33,300	–121	166,400	–106	46,500	–163	208,100	–651
	Cylinder 47				Cylinder 48				Cylinder 49			
Applied	52,500	0	165,200	0	56,100	0	251,000	0	79,100	0	246,800	0
Band B	48,200	–201	156,400	–416	53,900	104	239,300	877	75,000	105	238,500	171
Band E	46,900	–122	155,400	–50	54,700	–81	246,700	559	77,500	64	237,000	474
	Cylinder 50				Cylinder 51				Cylinder 52			
Applied	49,200	0	106,700	0	50,500	0	165,000	0	64,100	0	174,000	0
Band B	44,000	53	95,400	24	50,100	–220	160,000	–420	51,600	–82	137,700	–273
Band F	44,900	–16	99,900	242	51,800	–183	164,500	–630	52,700	0	140,600	–113
	Cylinder 53				Cylinder 54				Cylinder 55			
Applied	50,400	0	161,000	0	50,500	0	353,000	0	70,800	0	218,200	0
Band B	45,500	–90	144,500	–214	47,400	–29	330,000	–533	65,200	256	199,400	–326
Band E	48,100	–156	150,500	–146	48,600	–38	334,000	–987	69,700	–28	207,200	–378
	Cylinder 56				Cylinder 57				Cylinder 58			
Applied	70,900	0	215,400	0	74,800	0	148,200	0	68,100	0	152,700	0
Band B	66,600	–330	200,700	–405	69,900	–238	139,300	–224	65,800	1193	141,600	1253
Band E	65,600	–231	202,000	751	(a)	(a)	(a)	(a)	67,000	1097	145,400	1116
	Cylinder 59				Cylinder 60				Cylinder 61			
Applied	72,200	0	211,300	0	69,500	0	216,800	0	75,000	0	215,400	0
Band B	66,400	–214	196,300	–706	71,400	–106	216,000	–360	75,400	30	193,700	–210
Band E	66,700	–173	197,400	–307	71,000	42	213,100	326	71,800	–14	196,400	210

[a]No data.

TABLE III - INSTABILITY DATA

[ϵ_{cr} obtained by extrapolating test data to maximum moment;
M_{cr} corrected for tare weight of loading arm;
GI, general instability; PI, panel instability;
P/GI, failure started by panel instability
and ended by general instability]

Cylinder	Experimental maximum strain, ϵ_{cr}	Experimental maximum moment, M_{cr} (in.-lb)	Λ	Type of failure
44	19.4×10^{-4}	273,000	241	GI
45	18.5	280,000	174	GI
46	24.9	354,500	38	GI
47	24.8	380,500	30	P/GI
48	23.0	337,500	76	GI
49	26.6	403,500	19	PI
50	23.4	251,500	180	GI
51	16.7	246,500	228	GI
52	19.9	486,500	830	GI
53	14.2	508,500	344	GI
54	16.0	553,500	612	GI
55	16.8	553,300	725	GI
56	20.2	401,900	16	P/GI[1]
57	15.9	376,500	21	P/GI[2]
58	20.0	460,600	35	P/GI
59	20.3	451,000	54	P/GI
60	19.0	451,000	16	PI
61	20.3	403,000	74	GI

[1]Bolt failed at ring-stringer intersection.
[2]Ring broke at buckling load.

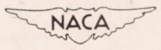

TABLE IV. – BEHAVIOR AFTER COLLAPSE

[All moments in in.-lb; all moments are corrected for tare weight of loading arm]

Cylinder	Maximum moment	Moment after collapse	Moment after increase in load	Moment after load dropped	Maximum moment after overnight rest	Moment after load dropped
44	273,000	267,000	273,000	268,000	277,000	248,000
45	280,000	276,000	287,000	263,000	287,000	257,000
46	354,500	297,500	-------	-------	302,500	294,500
47	380,500	360,500	354,500	350,500	300,500	262,500
48	337,500	320,500	331,500	308,500	313,500	298,500
49	403,500	387,500	-------	-------	383,500	341,500
50	251,500	227,500	-------	-------	237,500	206,100
51	246,500	238,500	-------	-------	251,500	219,500
52	486,500	459,500	-------	-------	521,500	487,500
53	508,500	484,500	-------	-------	529,500	505,500
54	553,500	434,500	-------	-------	459,500	-------
55	553,300	528,850	-------	-------	550,600	436,500
56	401,900	380,050	-------	-------	386,900	373,300
57	376,500	339,500	352,500	303,500	323,500	311,500
58	460,600	373,300	-------	-------	381,450	294,200
59	451,000	388,500	-------	-------	414,200	343,300
60	451,000	262,500	-------	-------	382,800	367,850
61	403,000	203,700	-------	-------	239,500	224,500

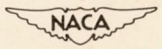

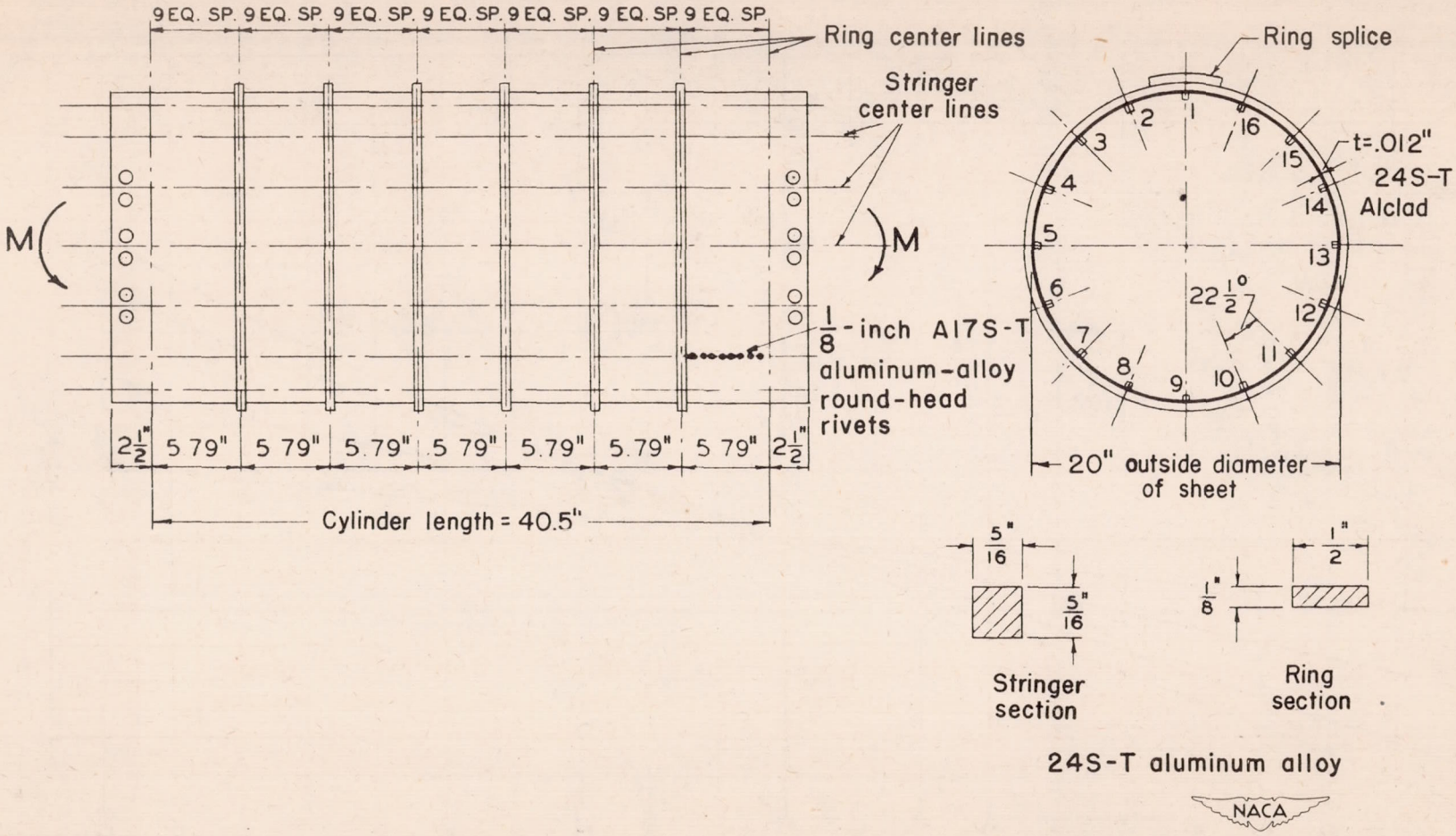

Figure 1.- Typical test specimen. Cylinder 50; 16 stringers.

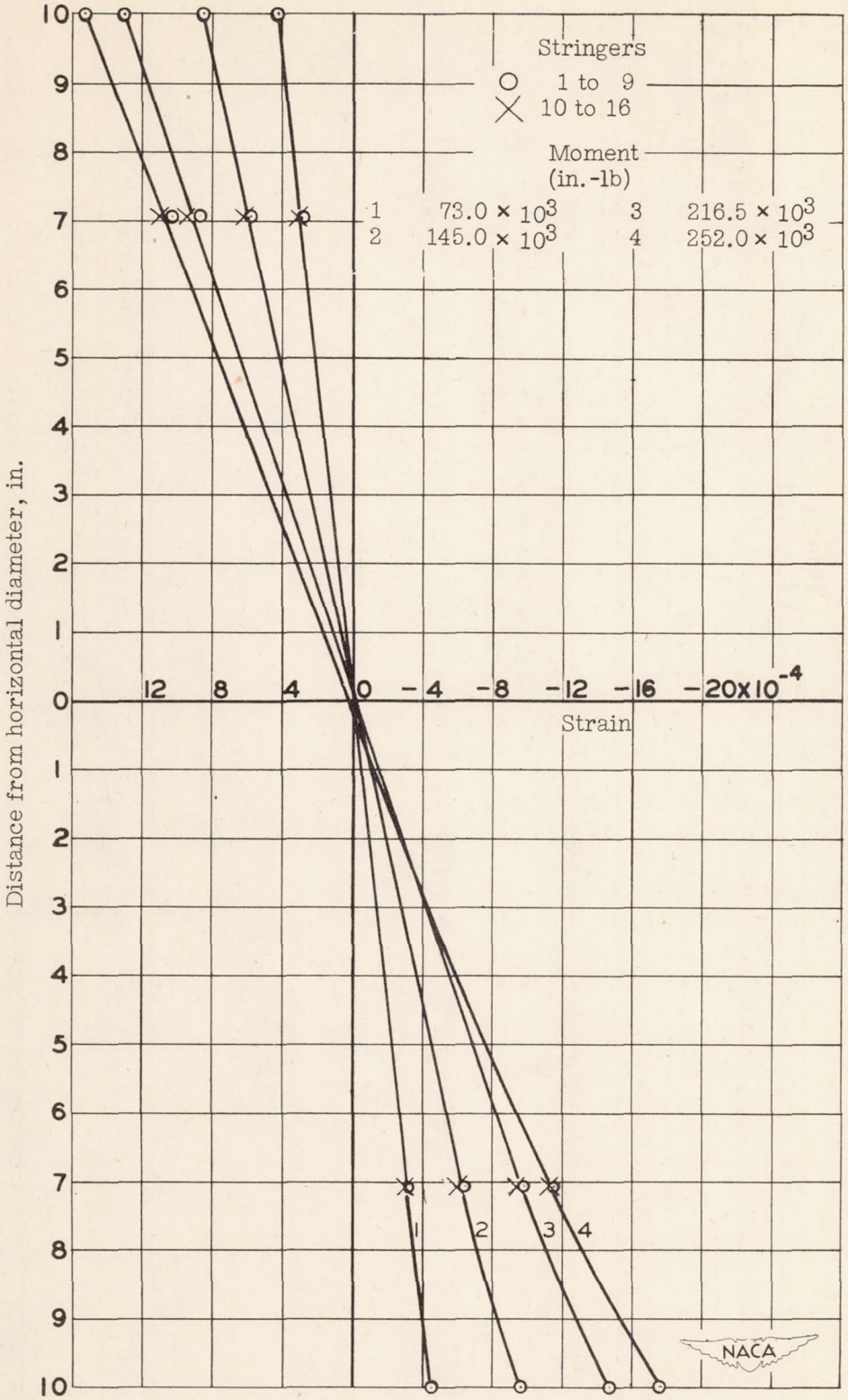

Figure 2.- Strain diagram of cylinder 44. Number of stringers, 16. Band B.

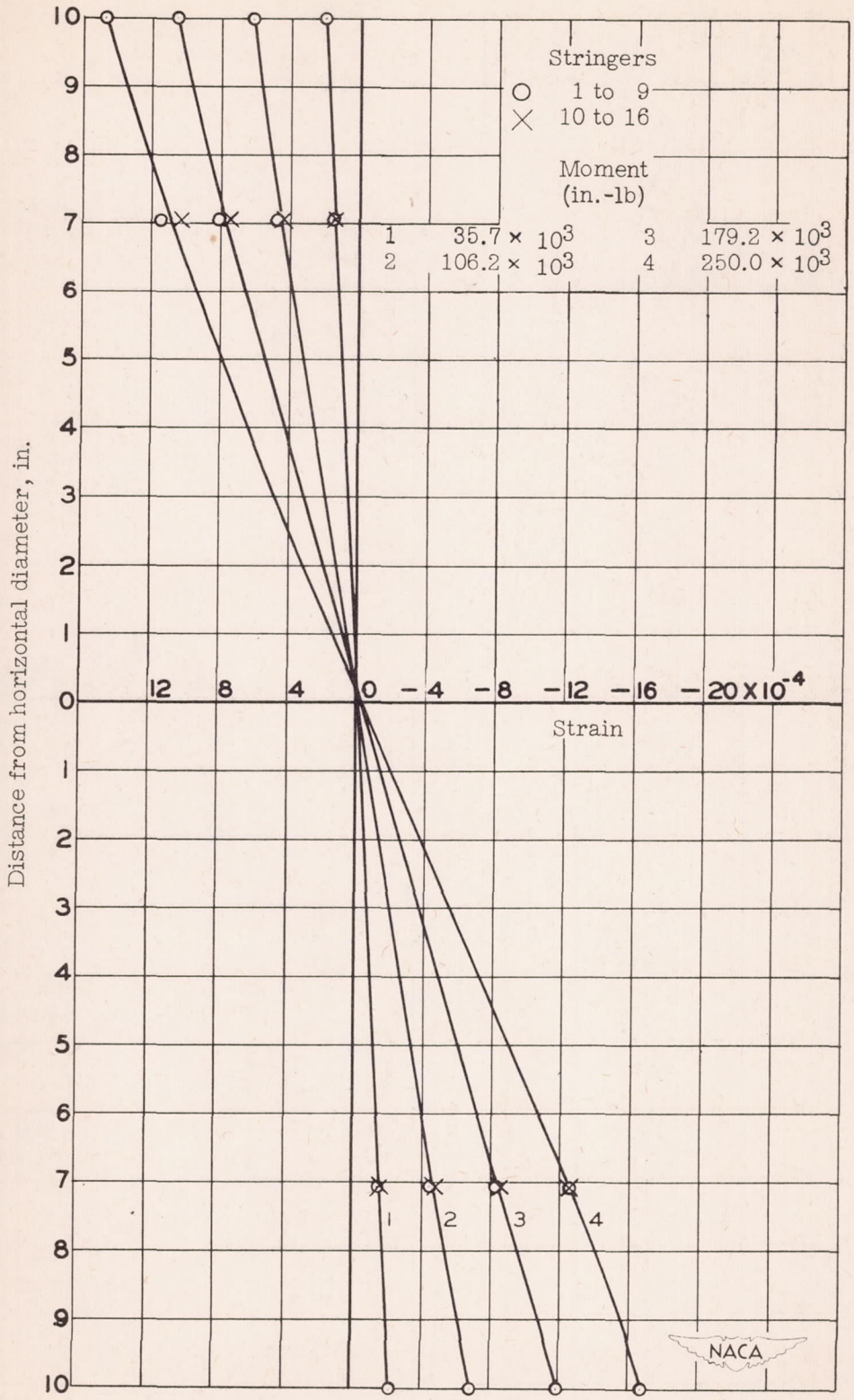

Figure 3.- Strain diagram of cylinder 45. Number of stringers, 16. Band E.

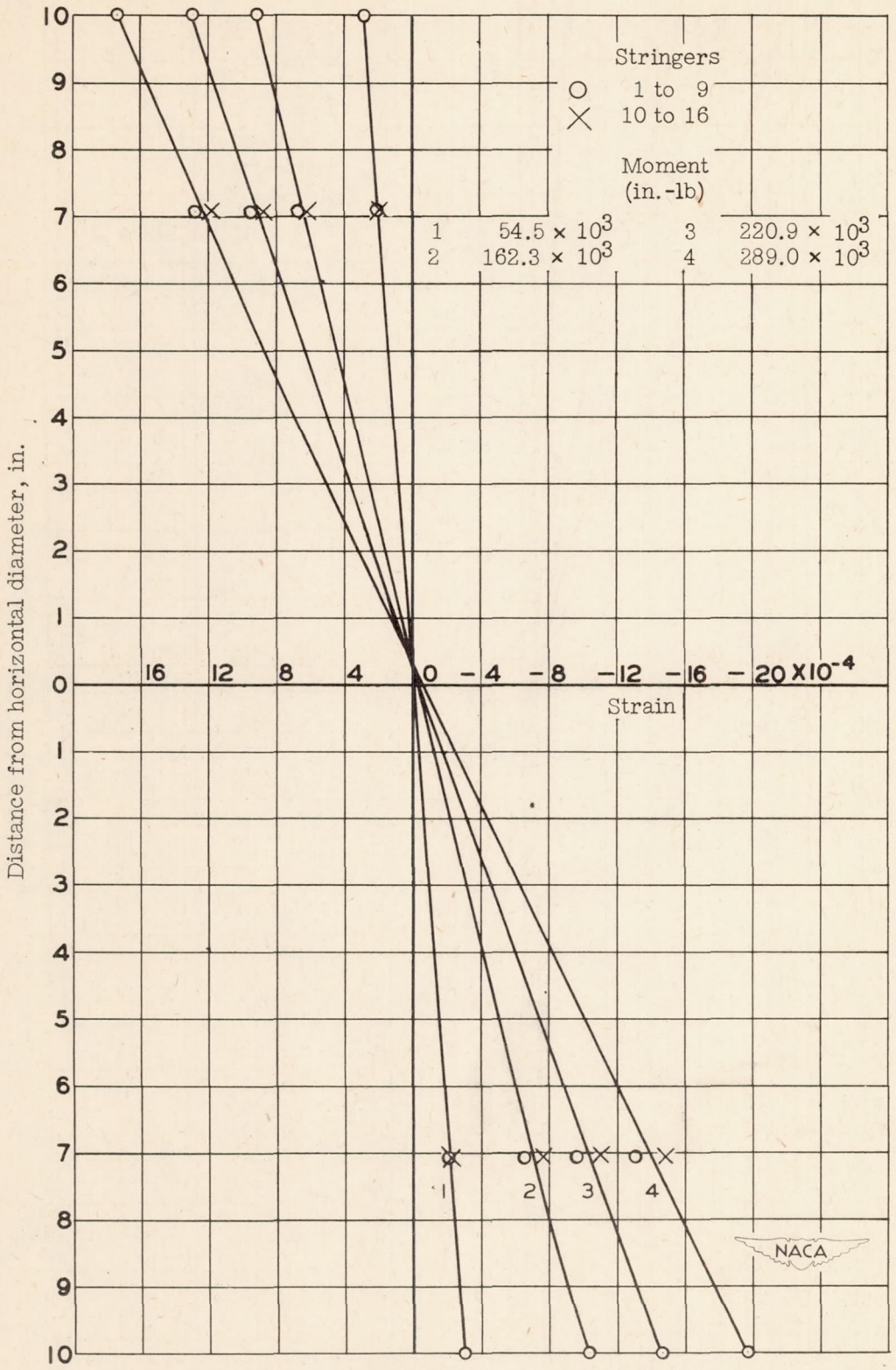

Figure 4.- Strain diagram of cylinder 46. Number of stringers, 16. Band B.

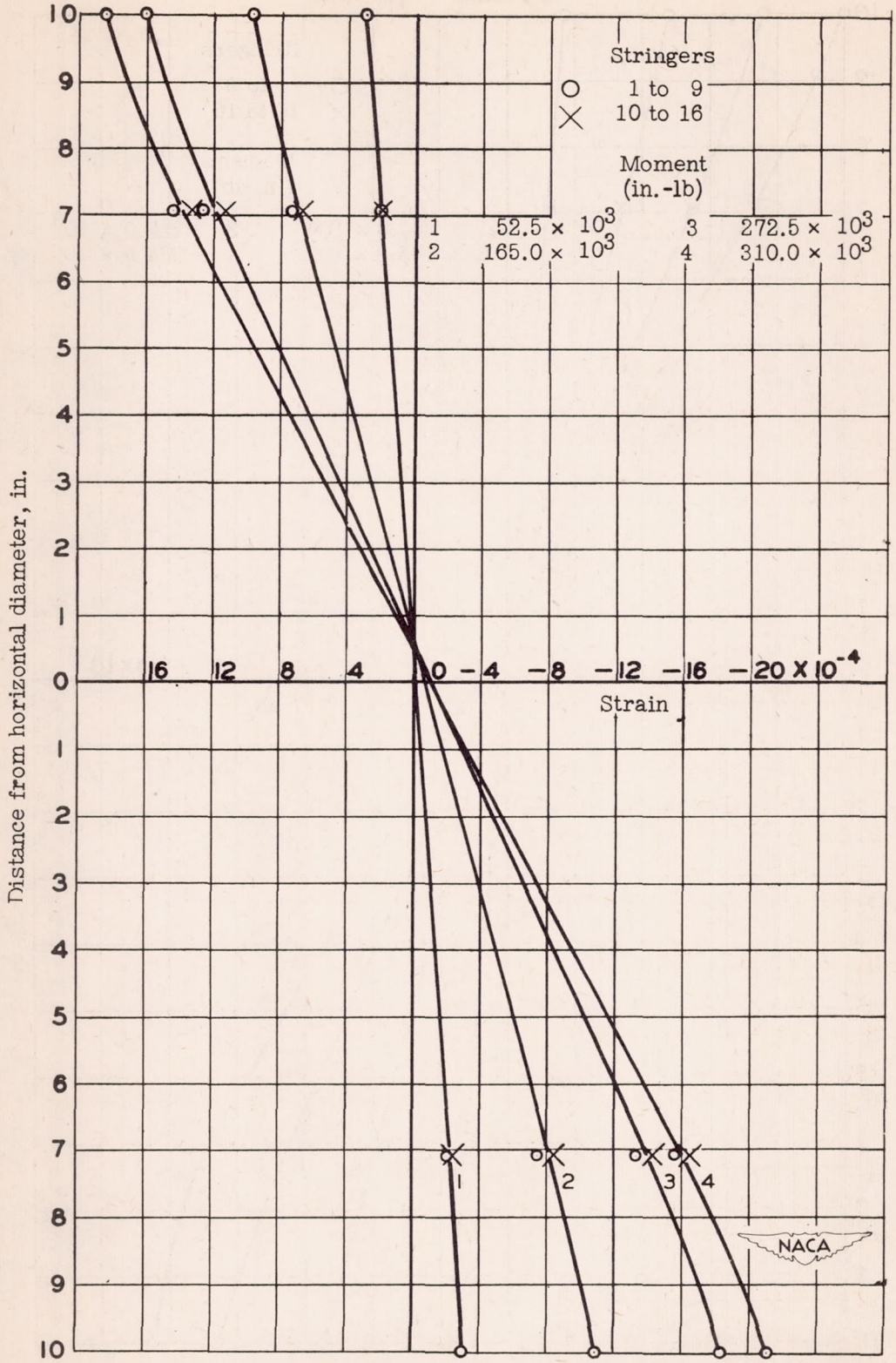

Figure 5.- Strain diagram of cylinder 47. Number of stringers, 16. Band B.

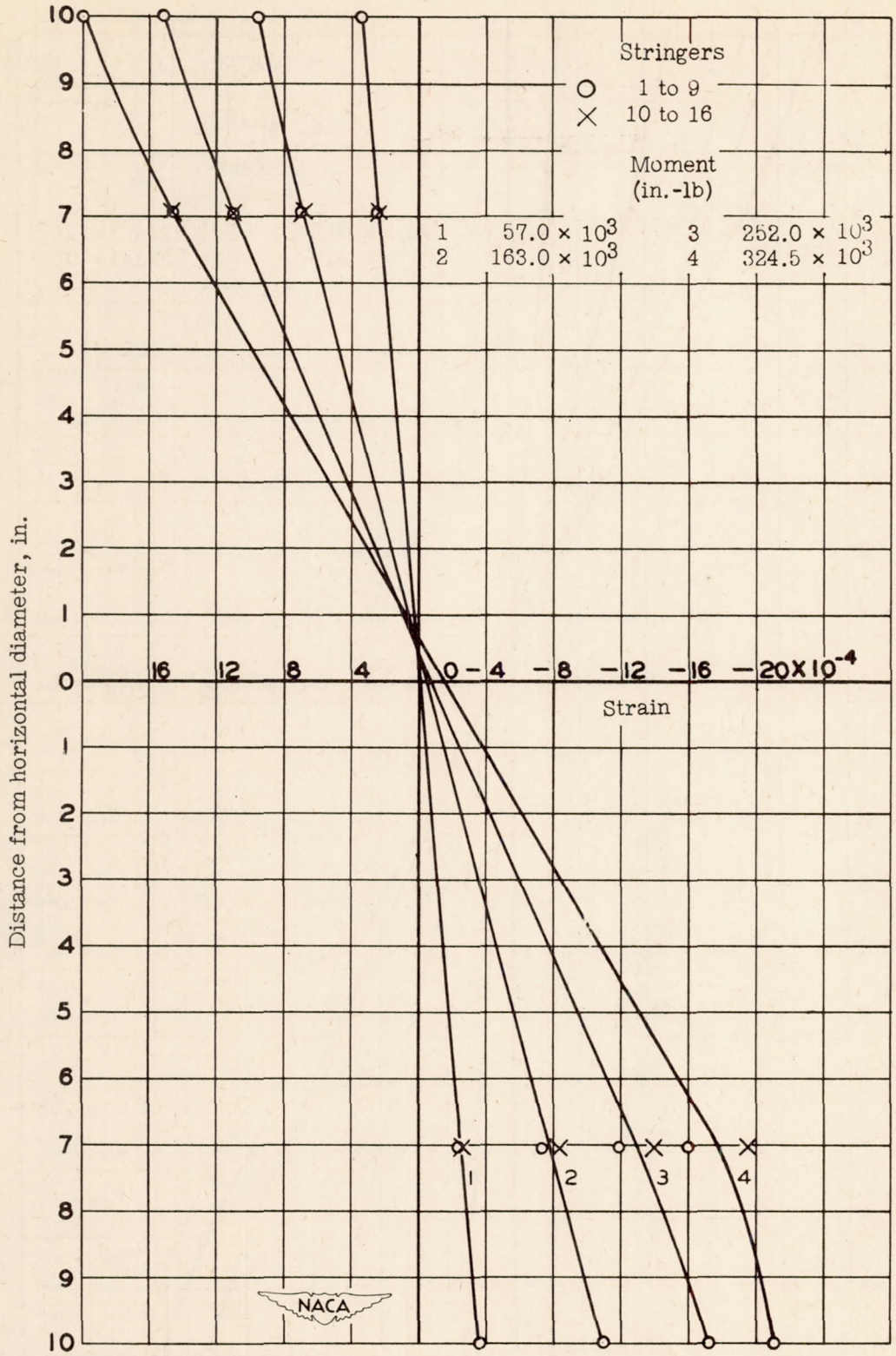

Figure 6.- Strain diagram of cylinder 48. Number of stringers, 16. Band E.

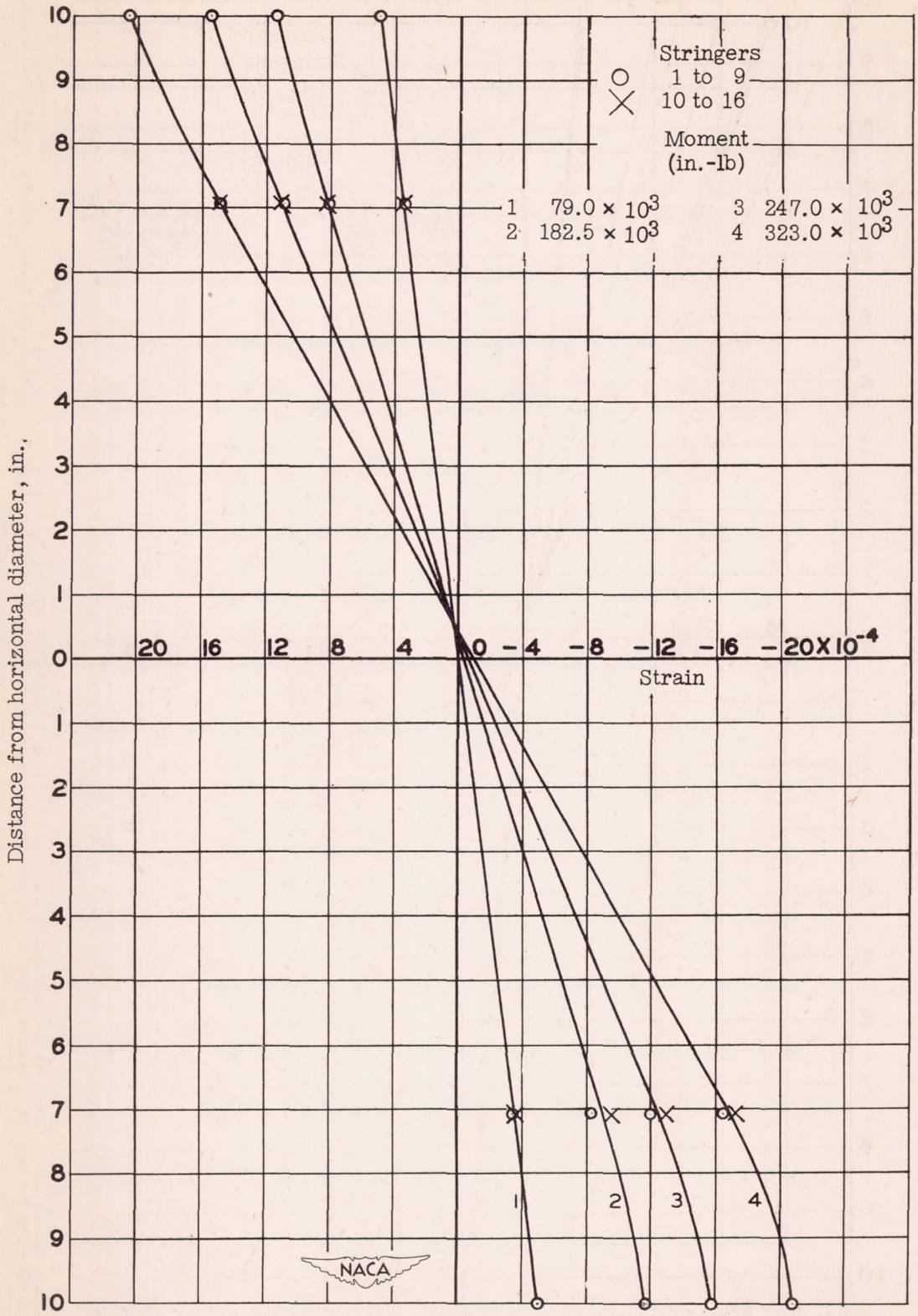

Figure 7.- Strain diagram of cylinder 49. Number of stringers, 16. Band E.

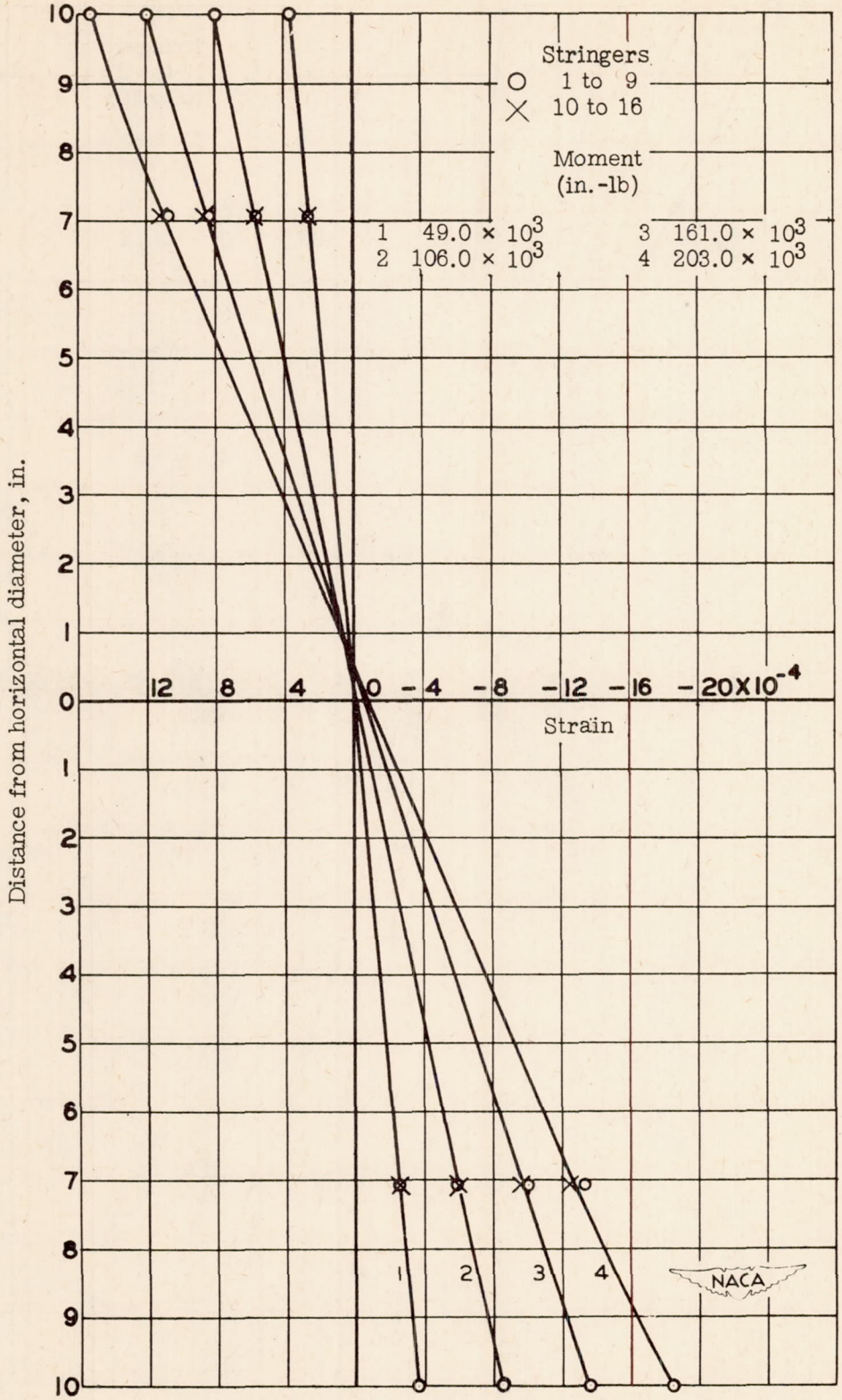

Figure 8.- Strain diagram of cylinder 50. Number of stringers, 16. Band B.

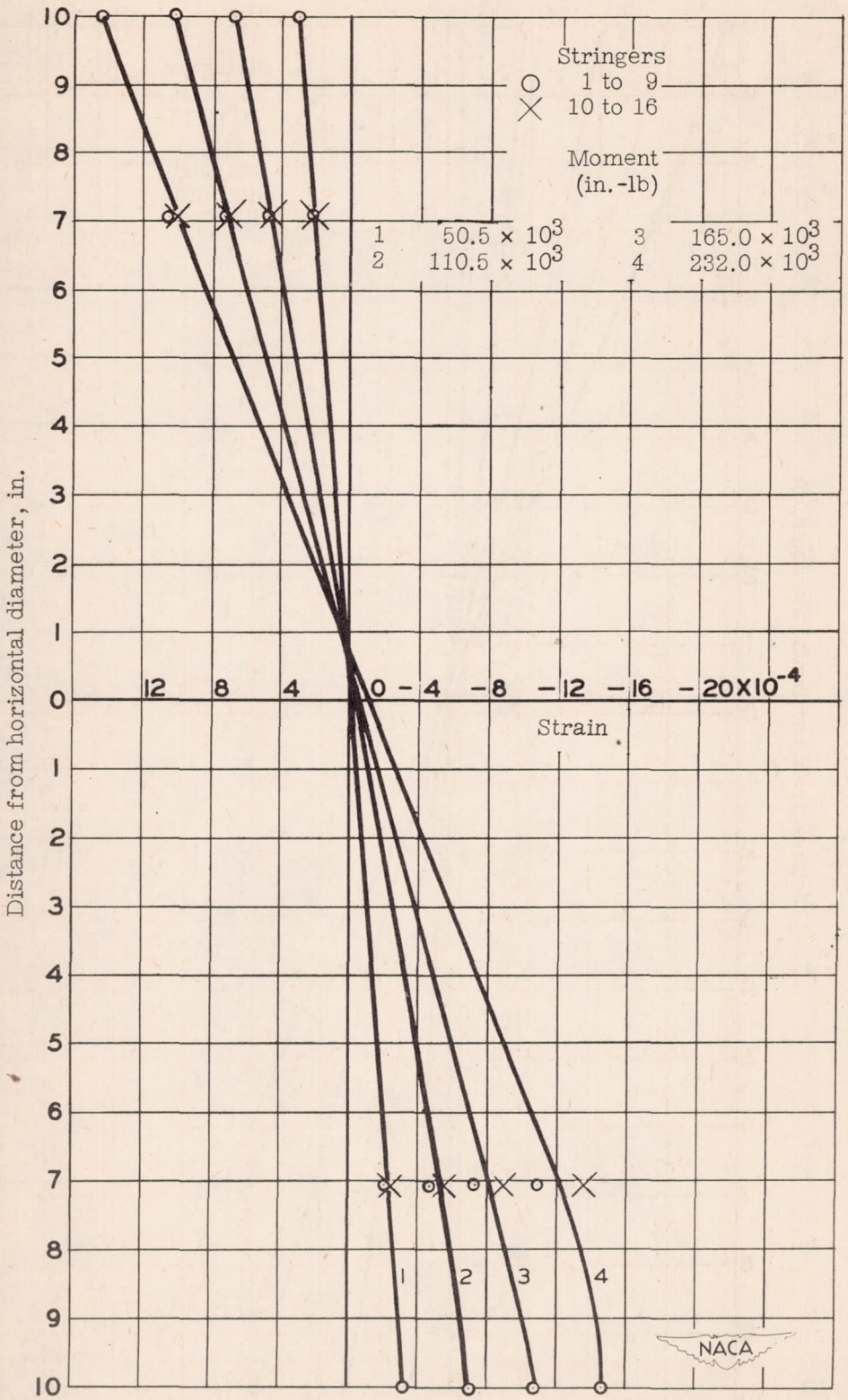

Figure 9.- Strain diagram of cylinder 51. Number of stringers, 16. Band B.

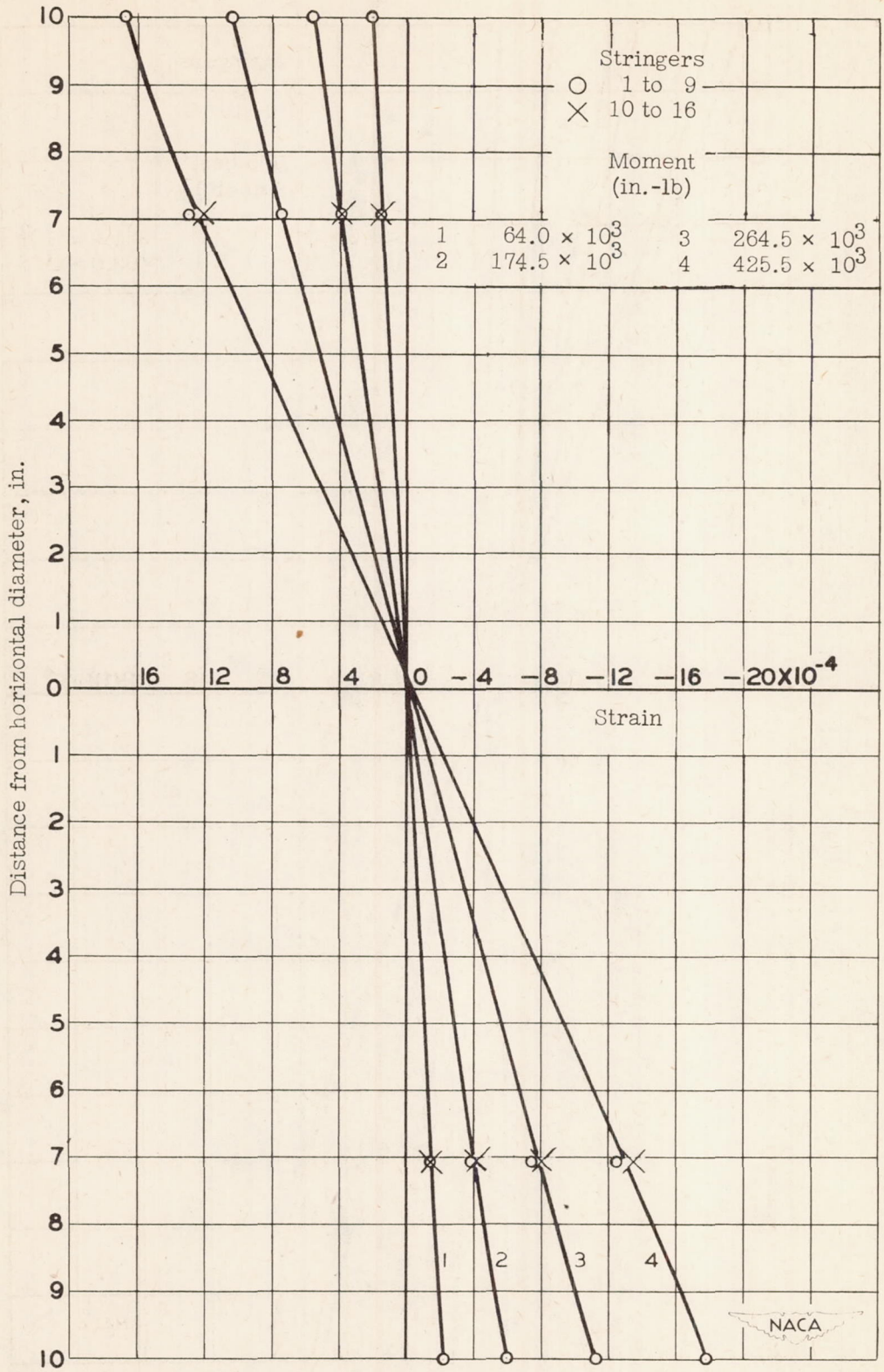

Figure 10.- Strain diagram of cylinder 52. Number of stringers, 16. Band F.

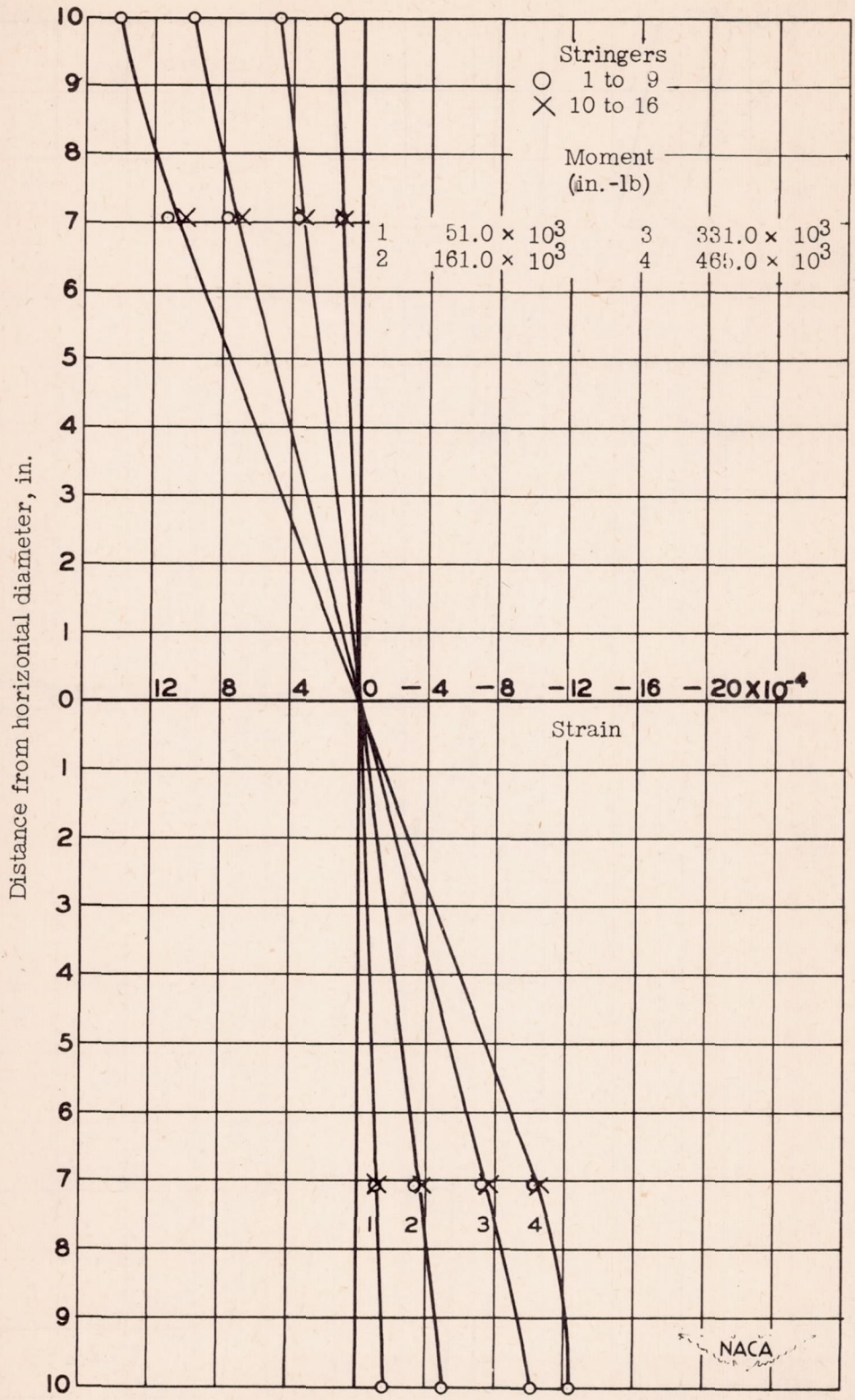

Figure 11.- Strain diagram of cylinder 53. Number of stringers, 16. Band B.

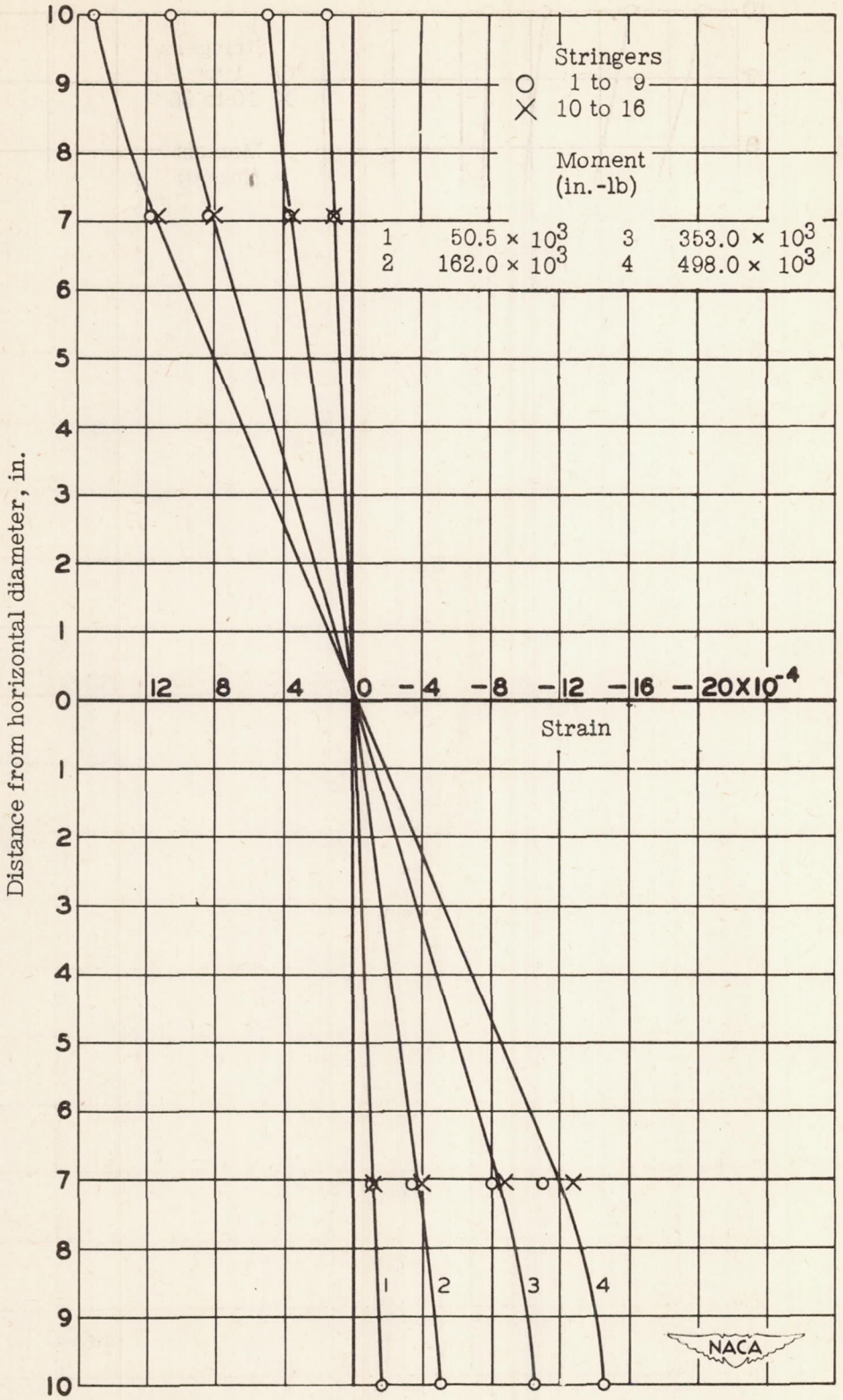

Figure 12.- Strain diagram of cylinder 54. Number of stringers, 16. Band B.

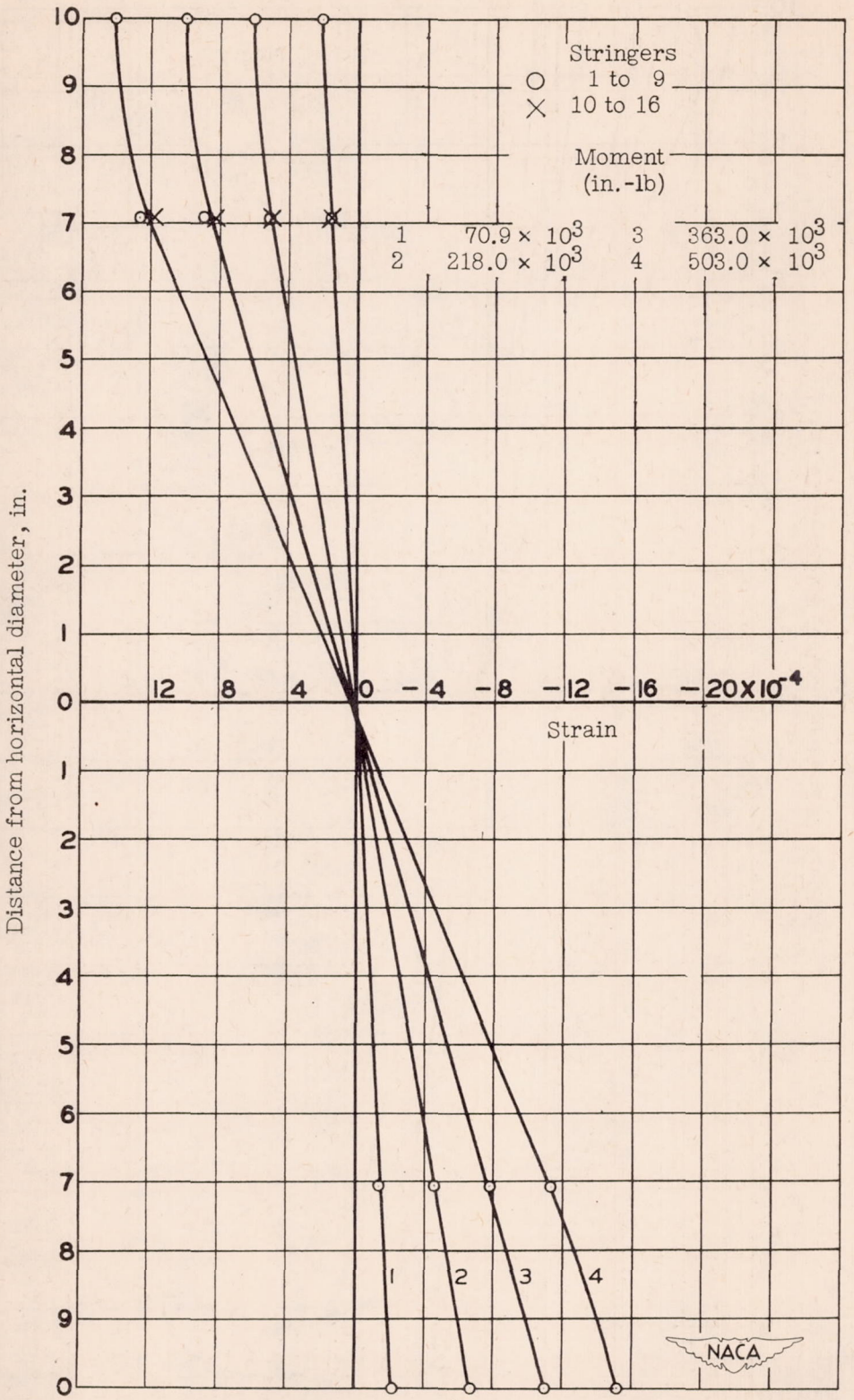

Figure 13.- Strain diagram of cylinder 55. Number of stringers, 16. Band B.

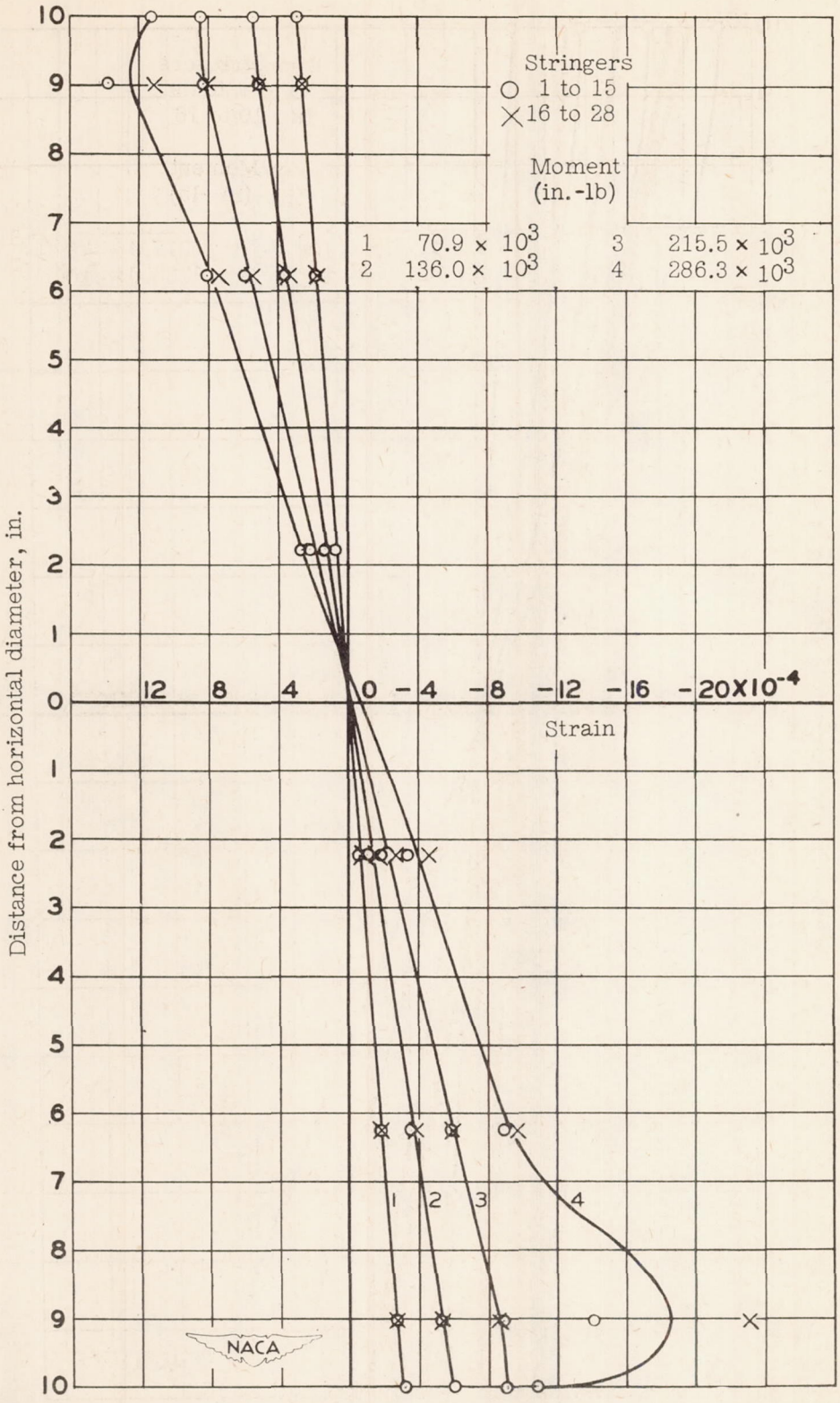

Figure 14.- Strain diagram of cylinder 56. Number of stringers, 28. Band B.

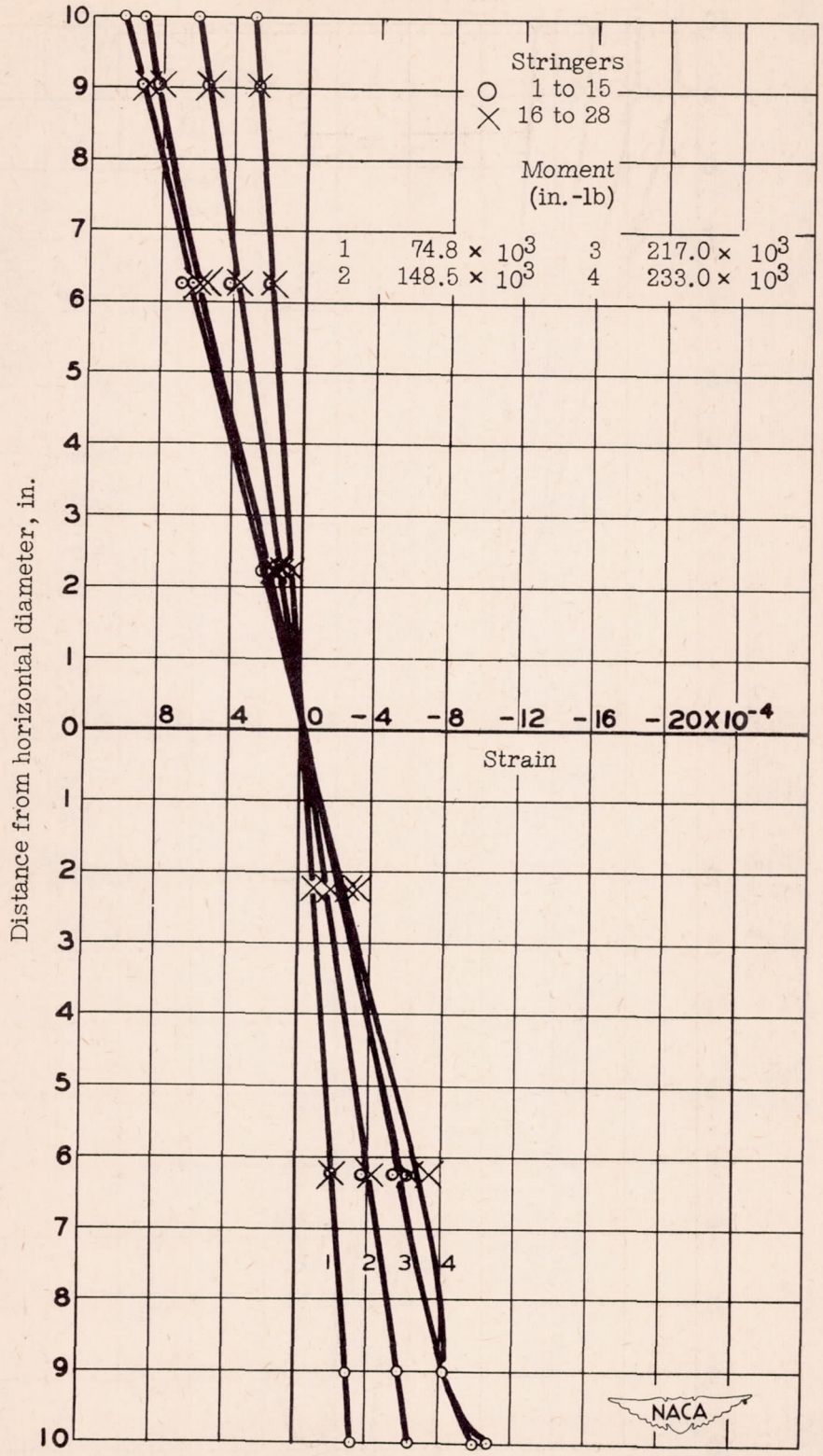

Figure 15.- Strain diagram of cylinder 57. Number of stringers, 28. Band B.

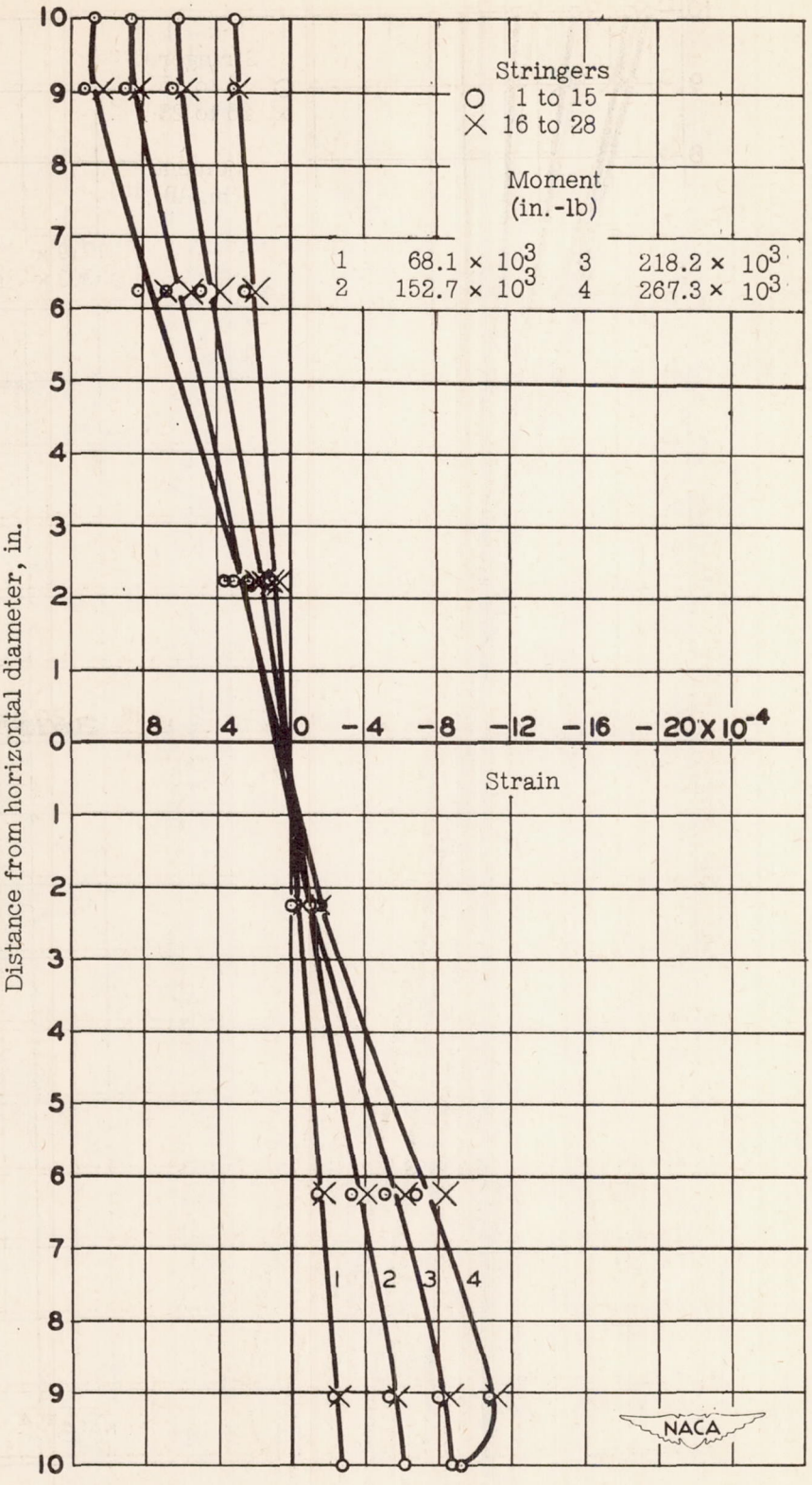

Figure 16.- Strain diagram of cylinder 58. Number of stringers, 28. Band B.

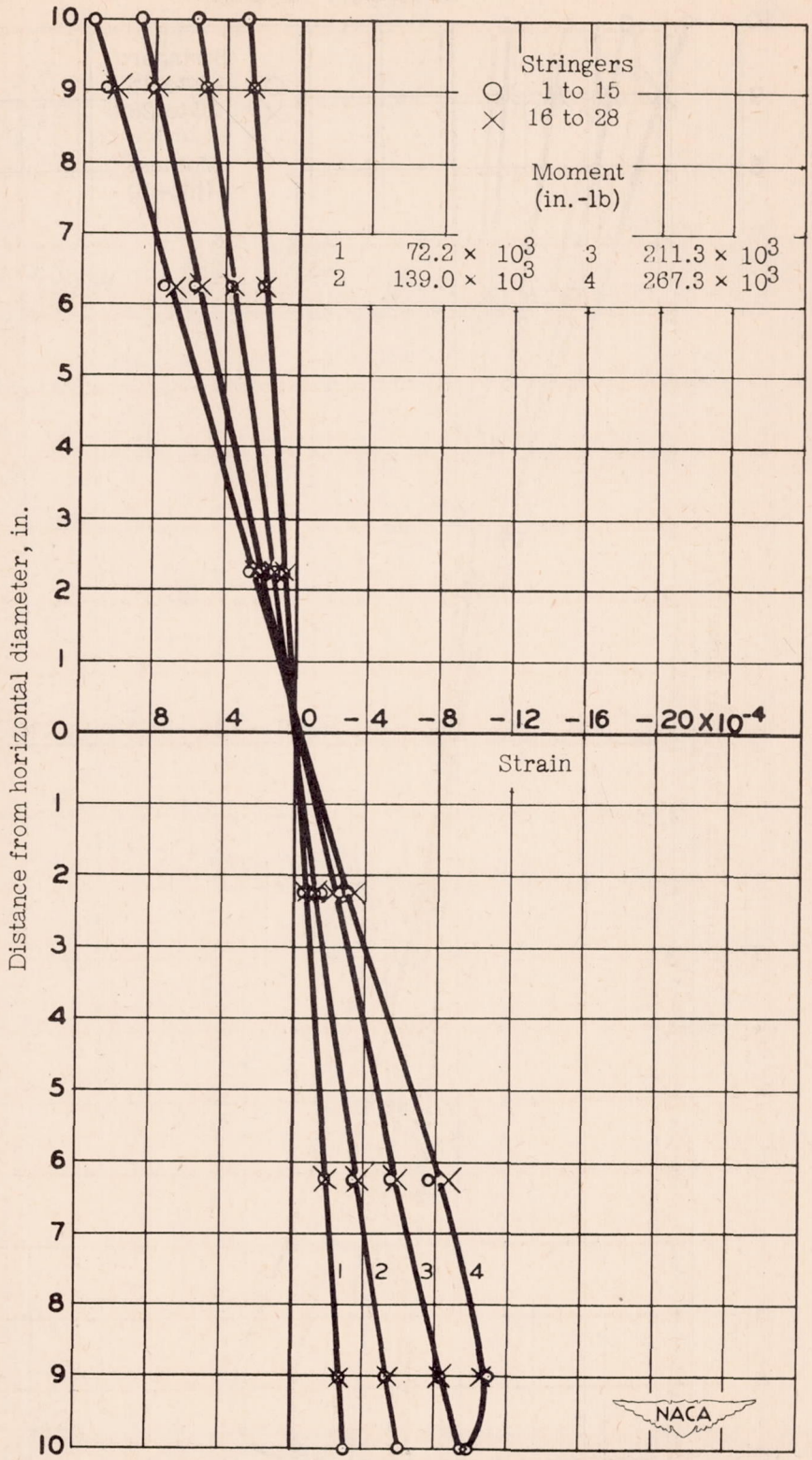

Figure 17.- Strain diagram of cylinder 59. Number of stringers, 28. Band E.

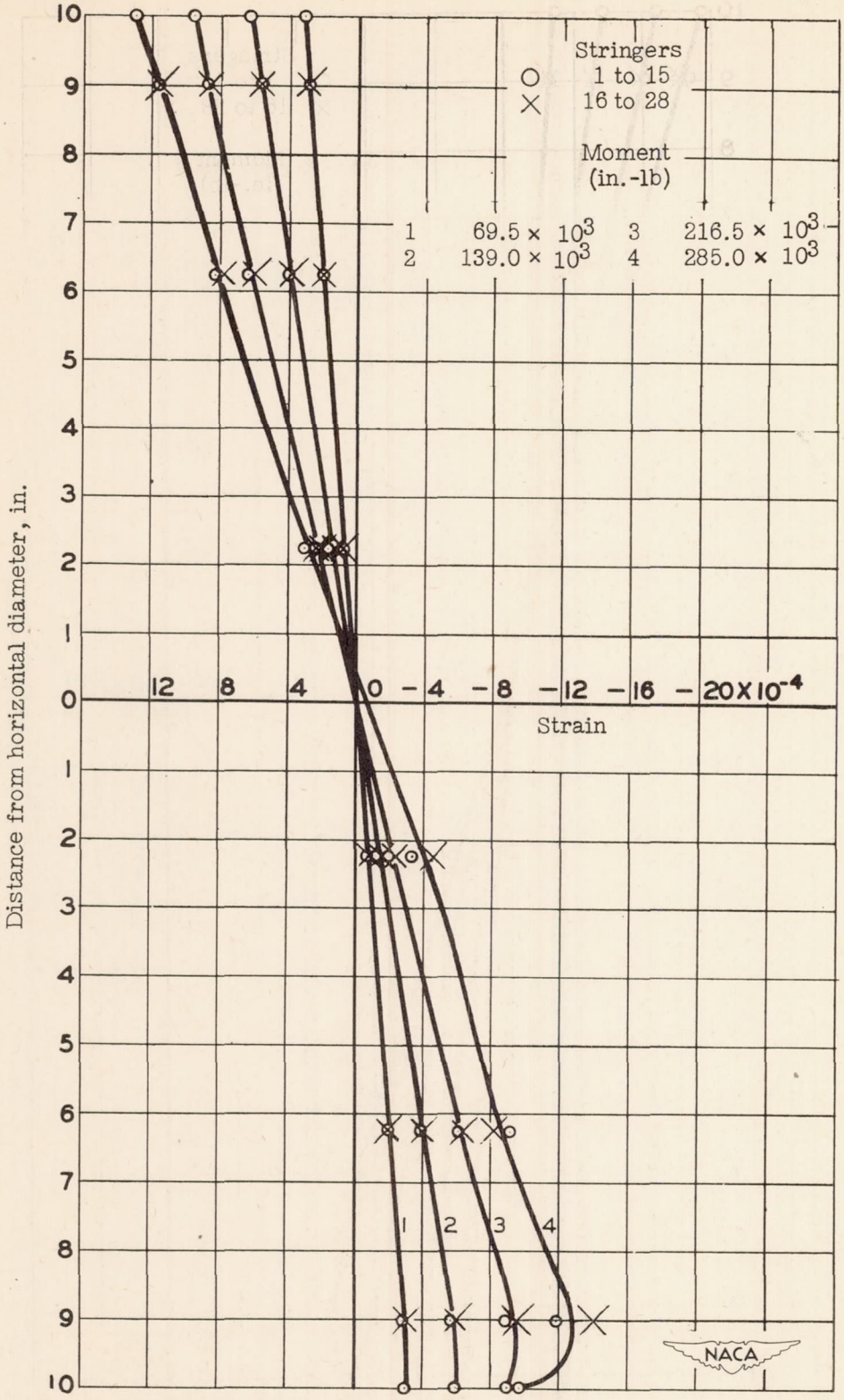

Figure 18.- Strain diagram of cylinder 60. Number of stringers, 28. Band E.

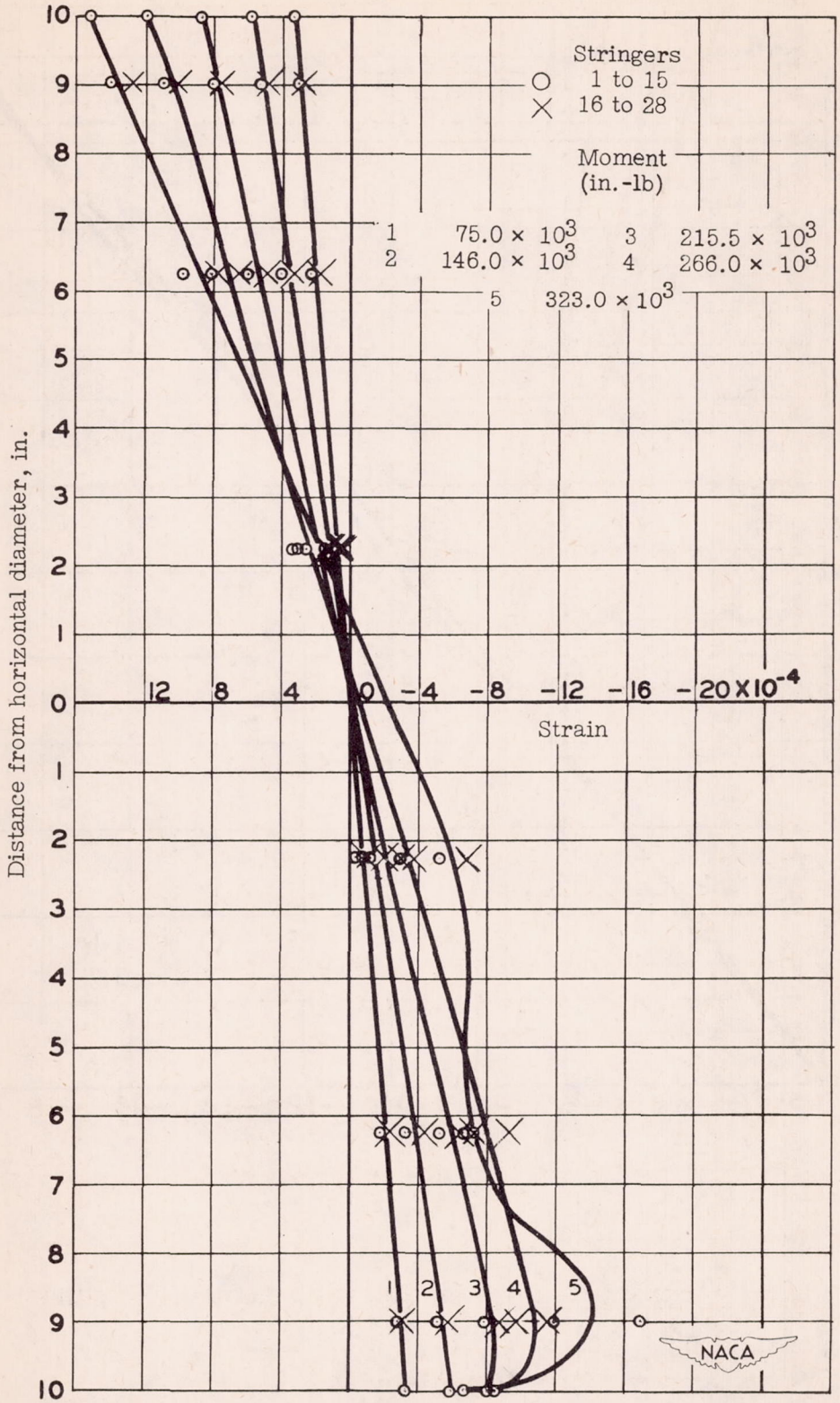

Figure 19.- Strain diagram of cylinder 61. Number of stringers, 28. Band B.

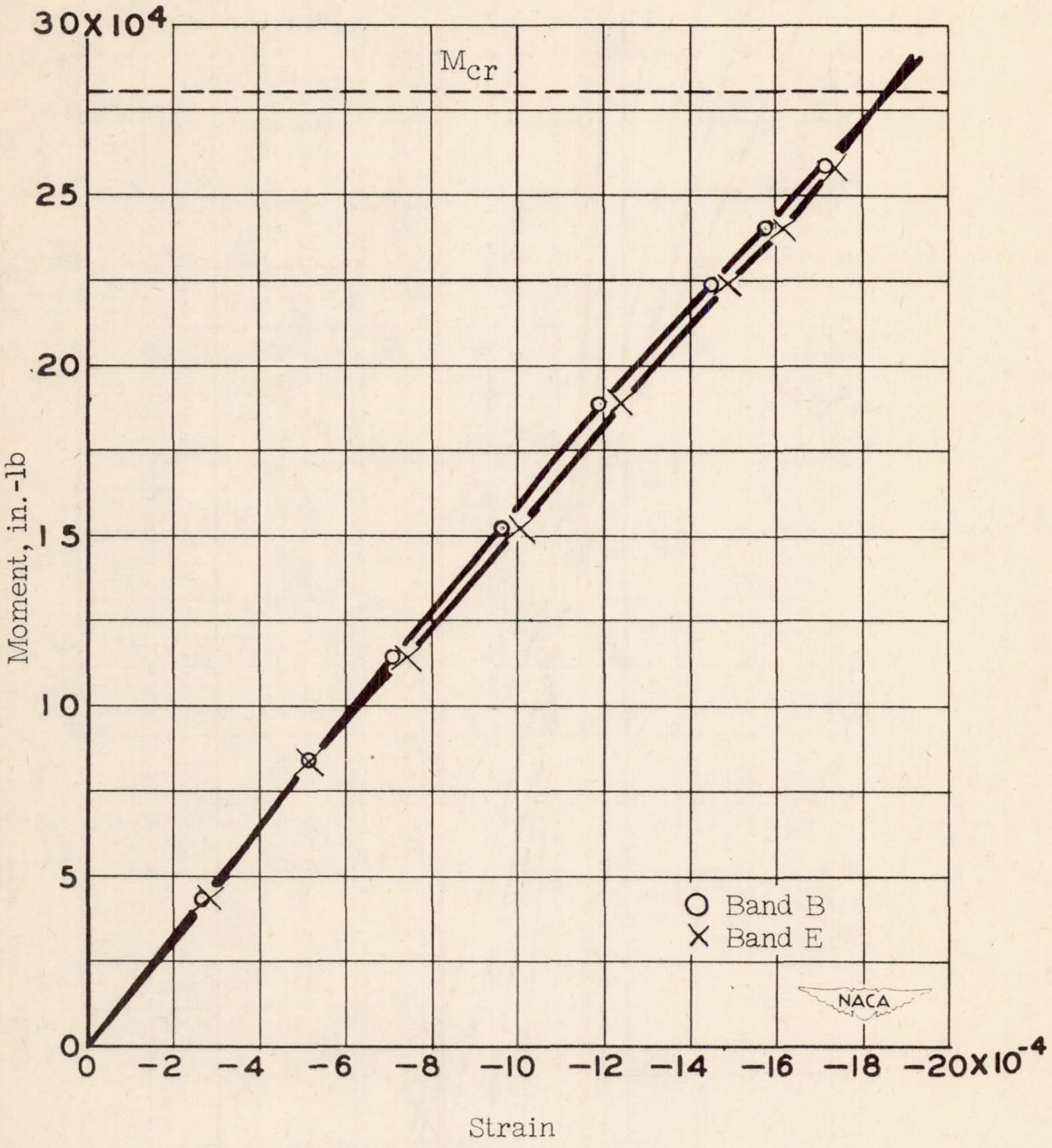

Figure 20.- Stringer strain variation with moment. Cylinder 45; stringer 9.

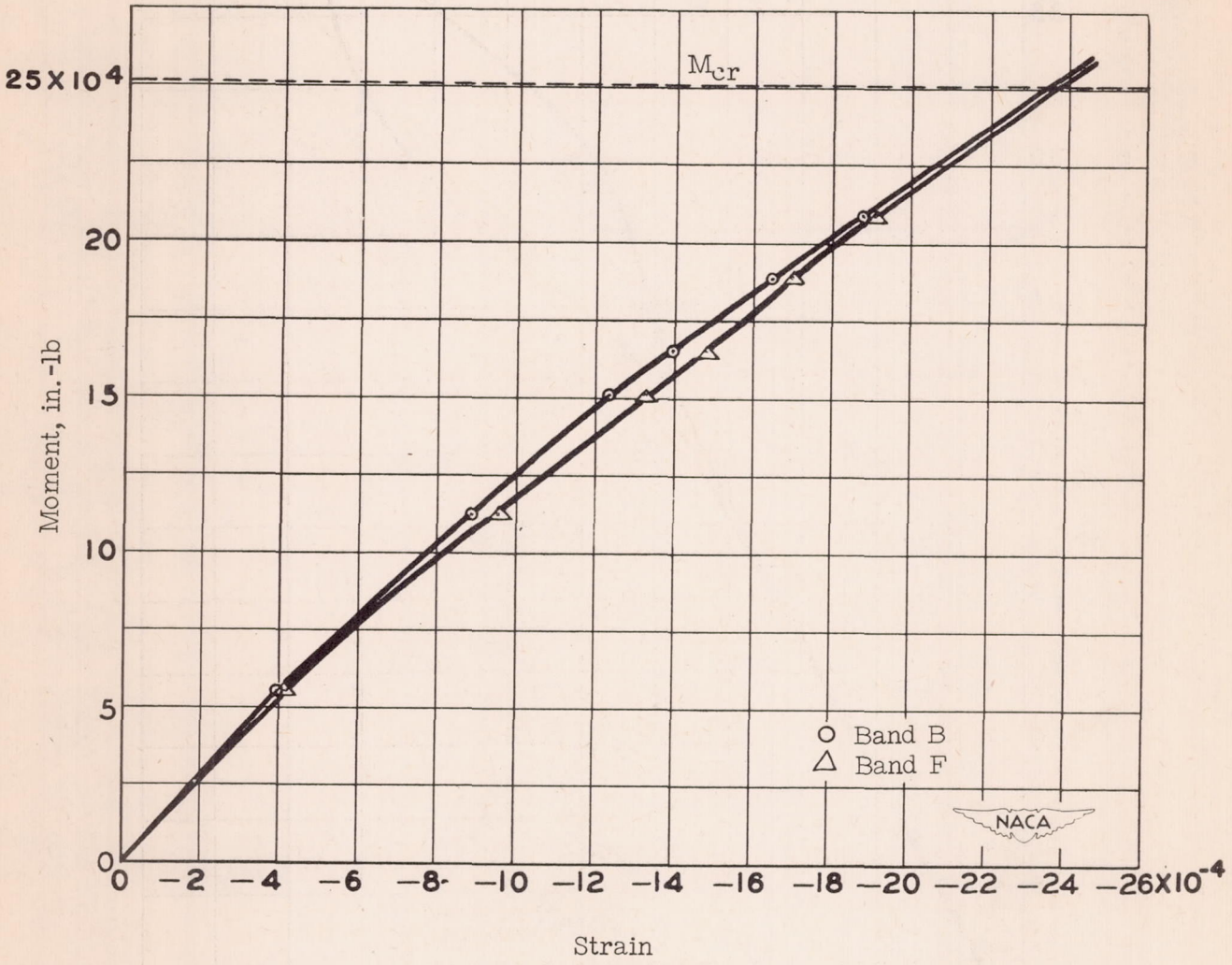

Figure 21.- Stringer strain variation with moment. Cylinder 50; stringer 9.

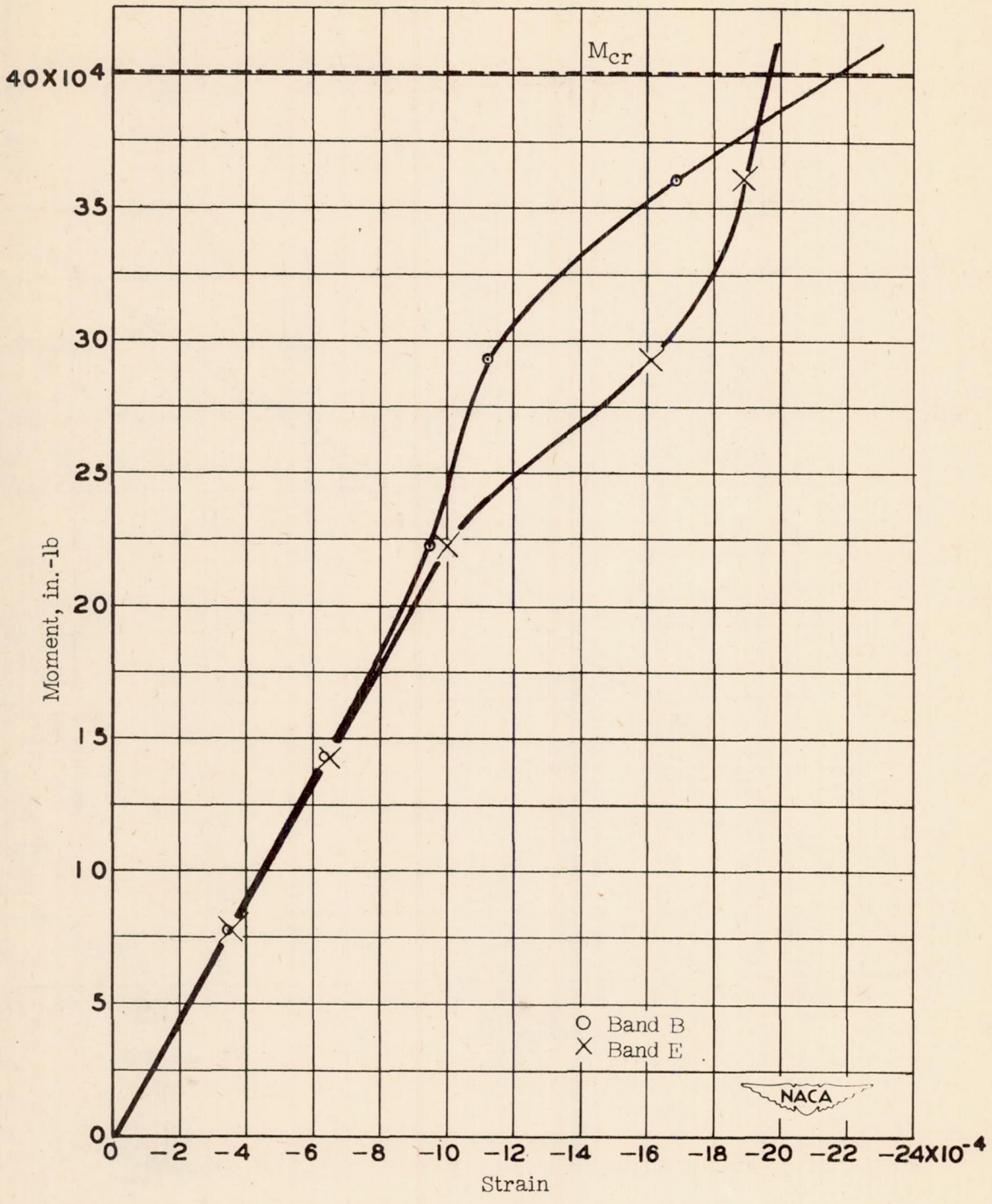

Figure 22.- Stringer strain variation with moment. Cylinder 56; stringer 15.

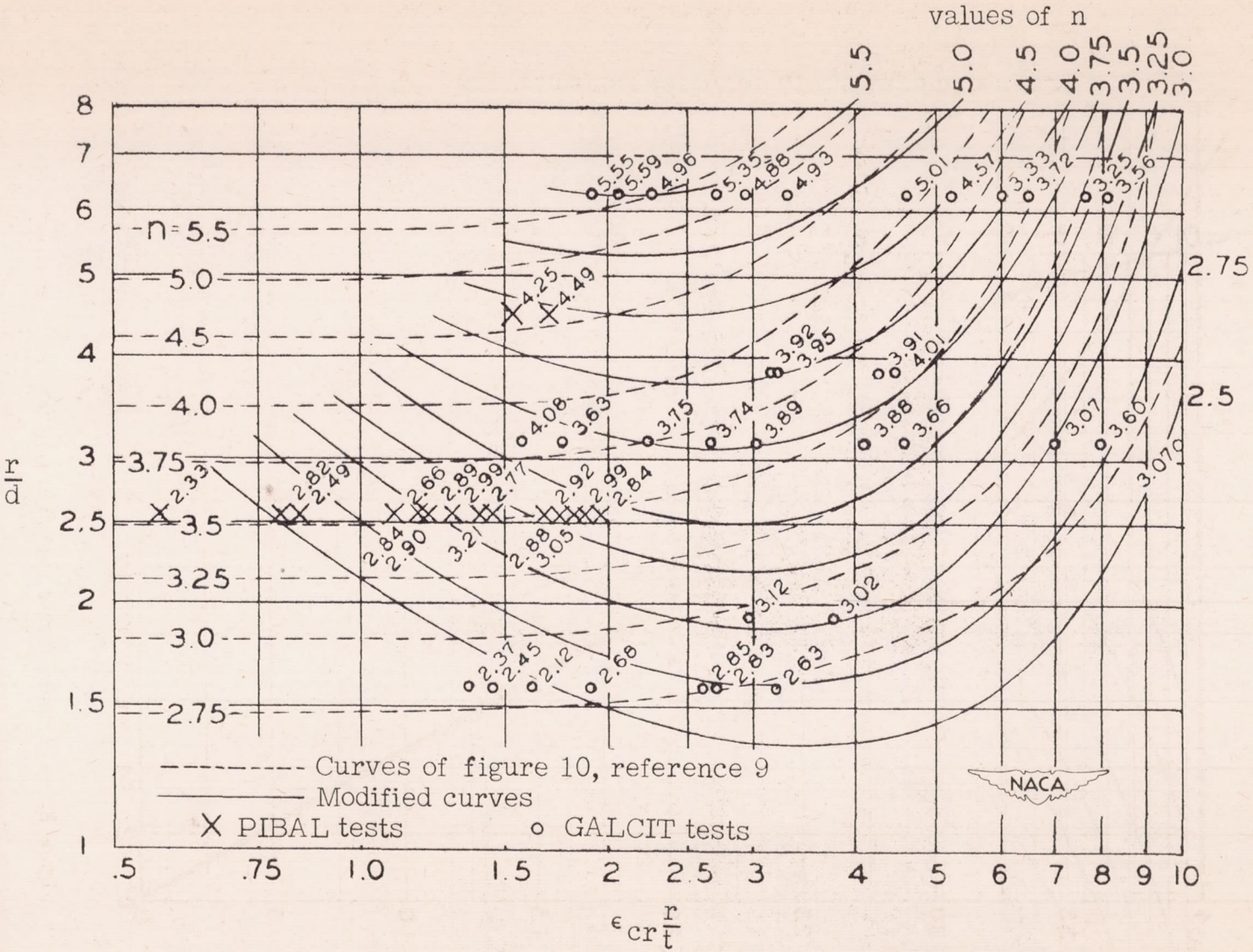

Figure 23.- Experimental variation of the parameter n. Comparison with curves of reference 9. Values of n given adjacent to plotted points.

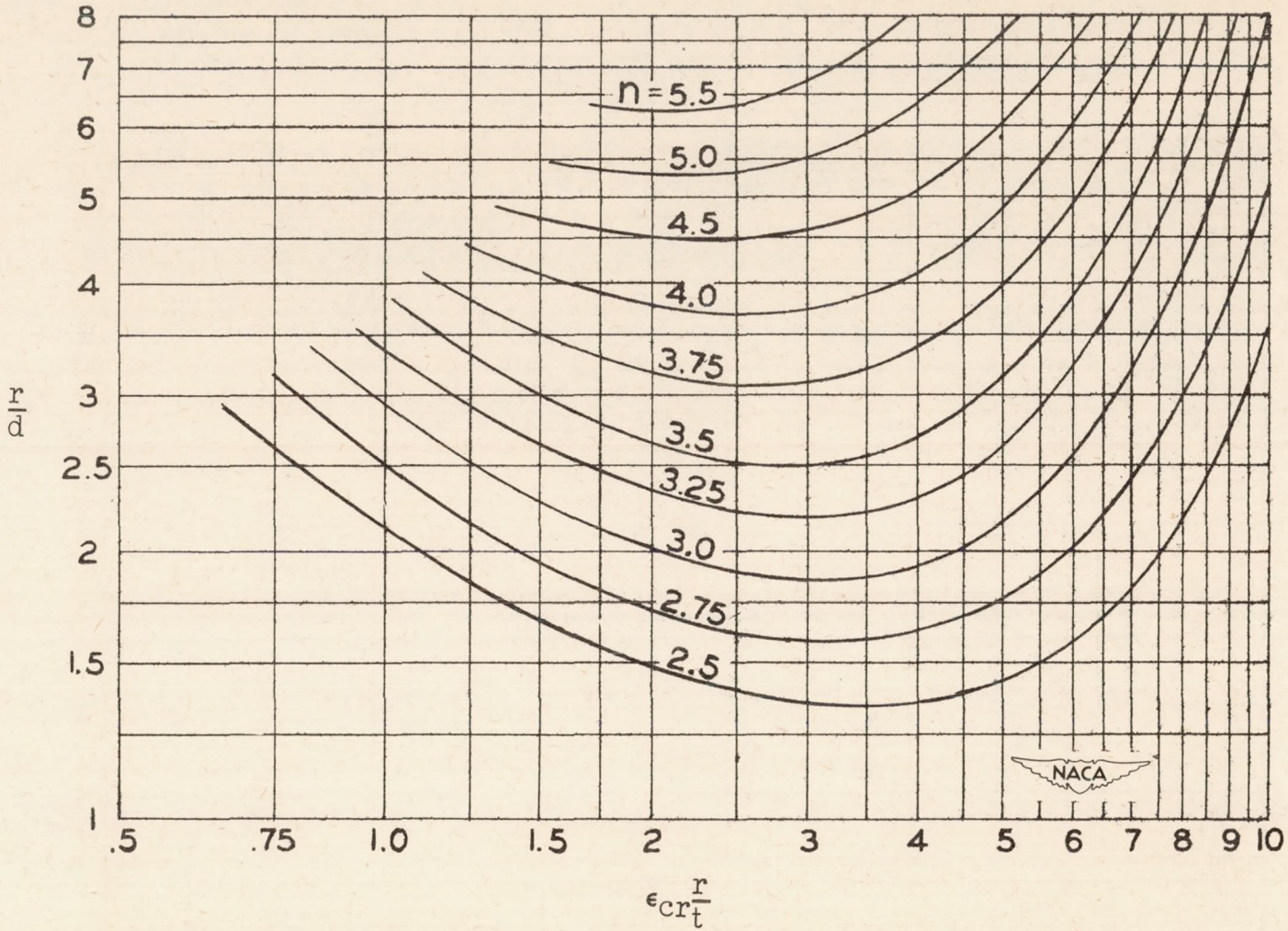

Figure 24.- Experimental variation of the parameter n.

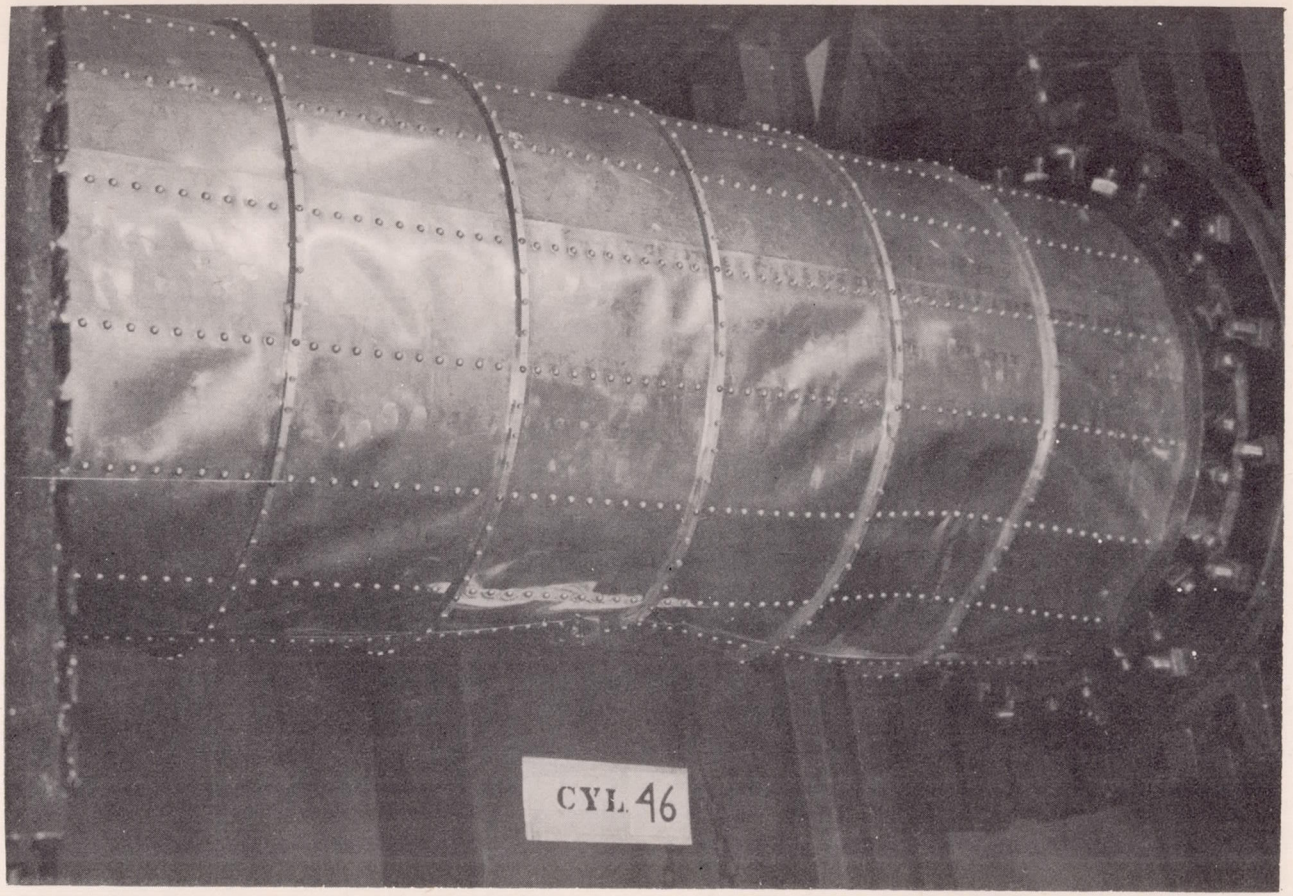

Figure 25.- Photograph of cylinder 46 after buckling.

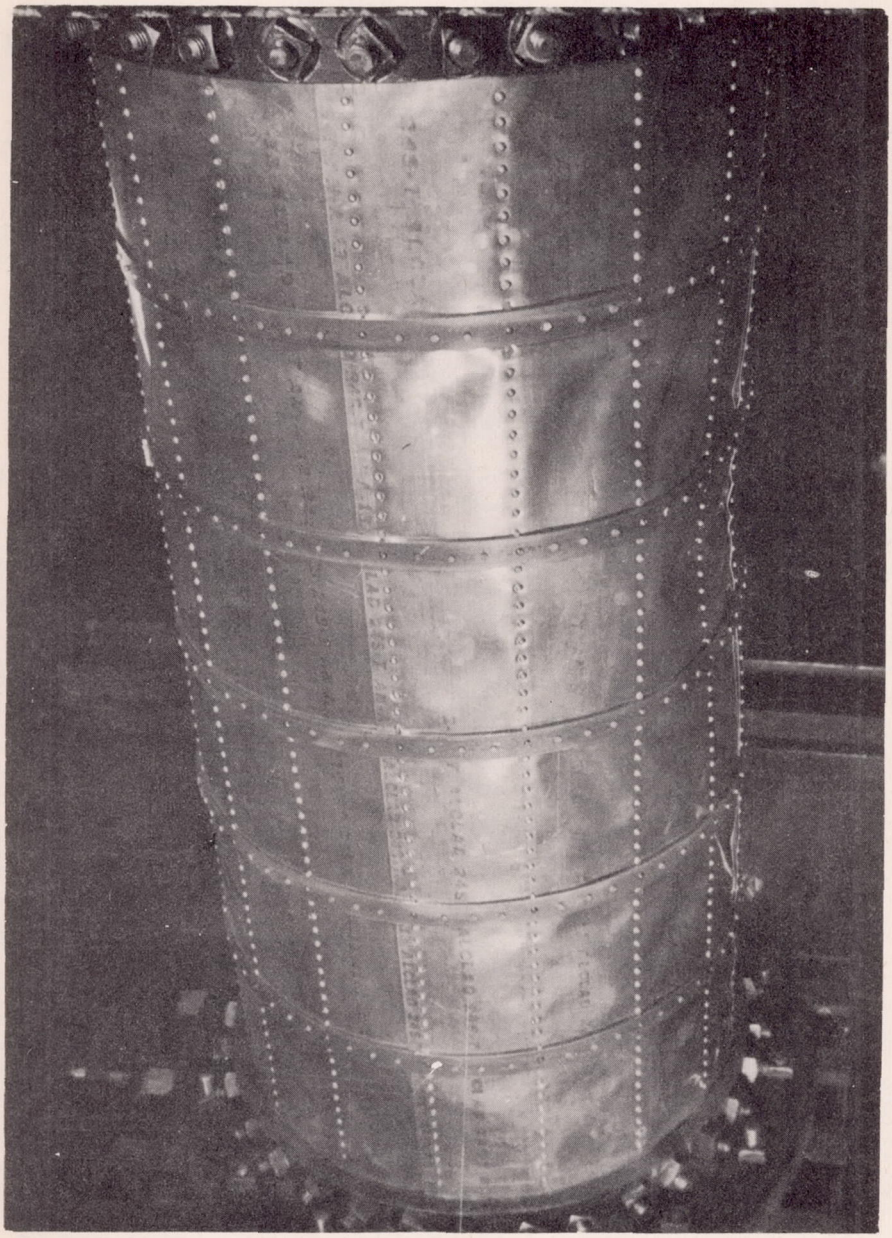

Figure 26.- Photograph of cylinder 47 after buckling.

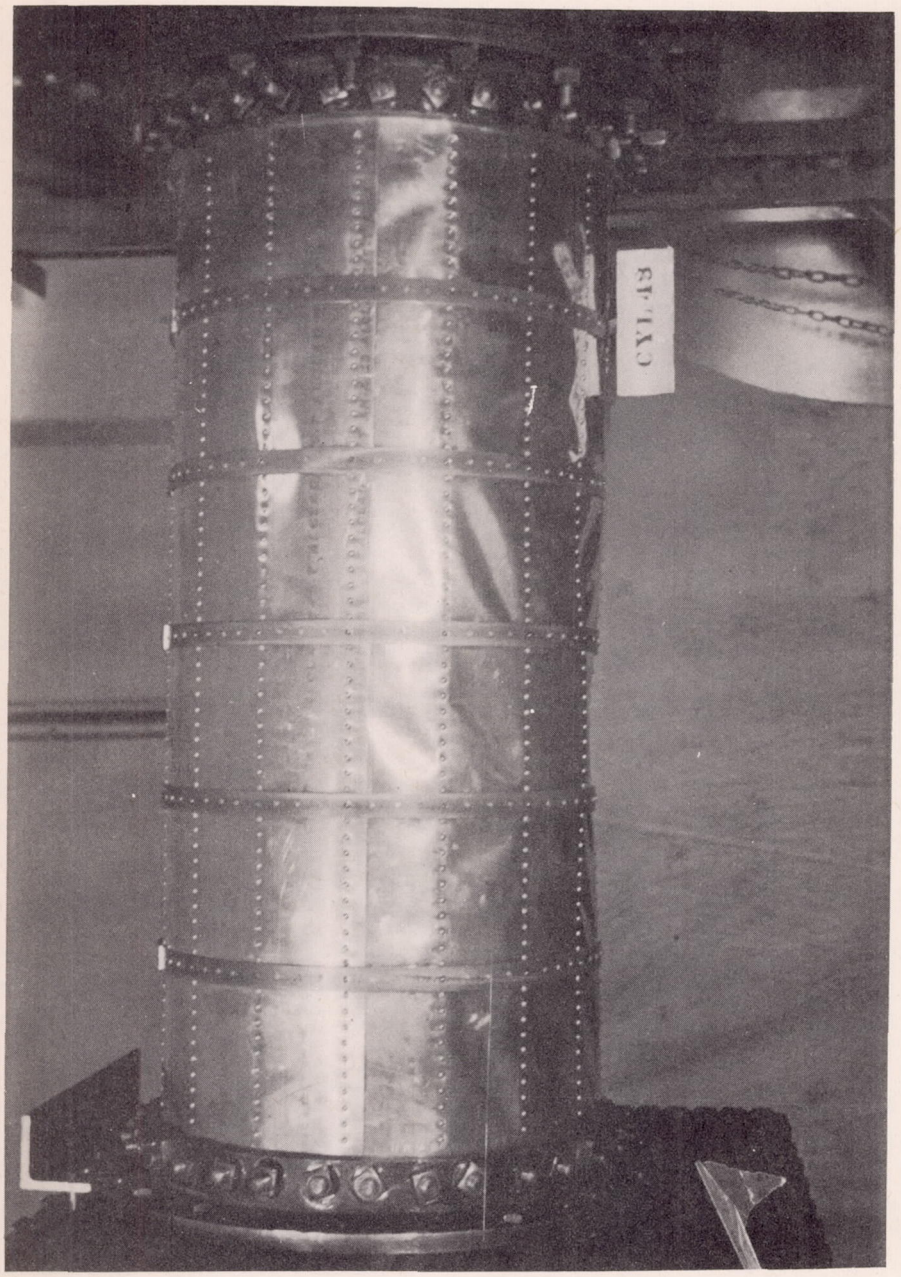

Figure 27.- Photograph of cylinder 48 after buckling.

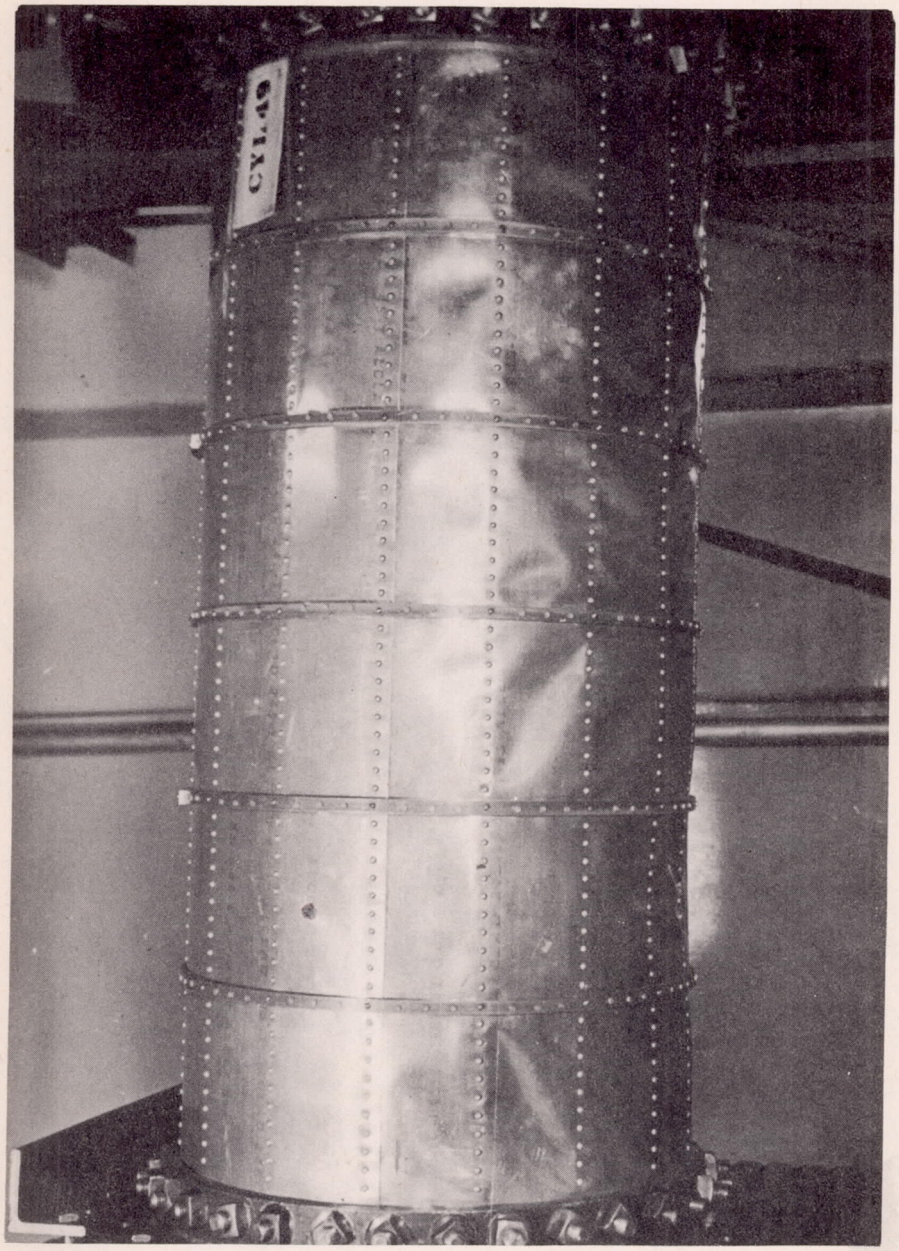

Figure 28.- Photograph of cylinder 49 after buckling.

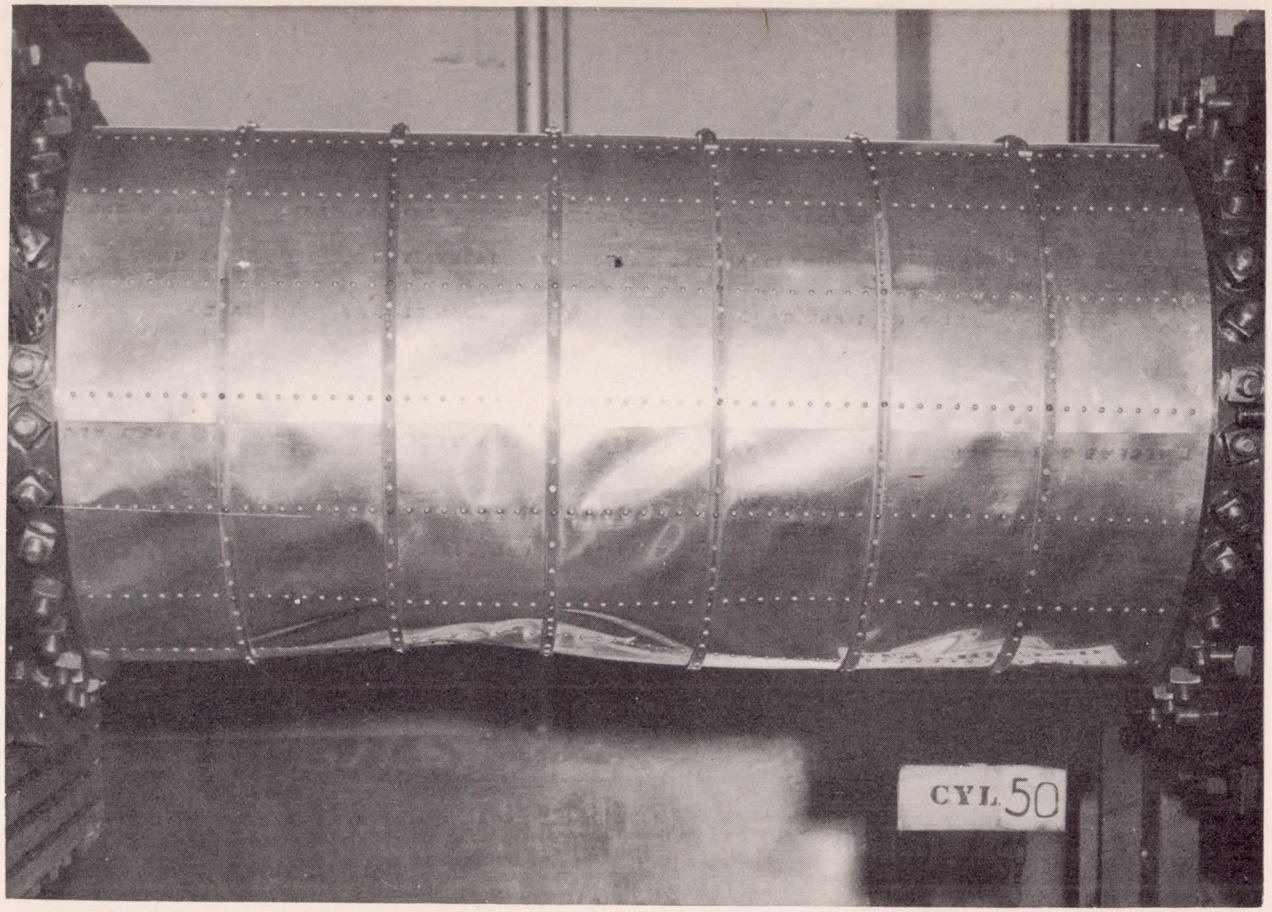

Figure 29.- Photograph of cylinder 50 after buckling.

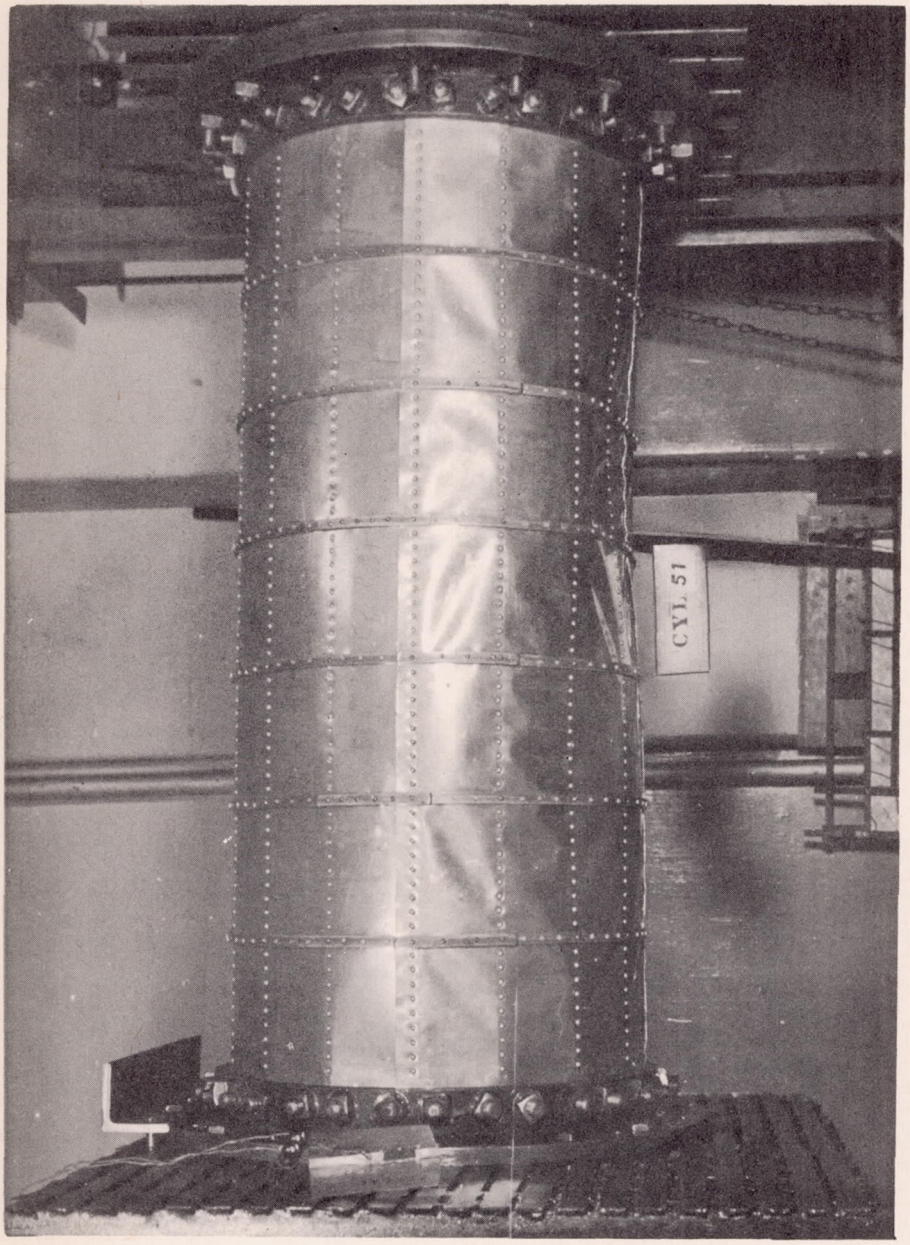

Figure 30.- Photograph of cylinder 51 after buckling.

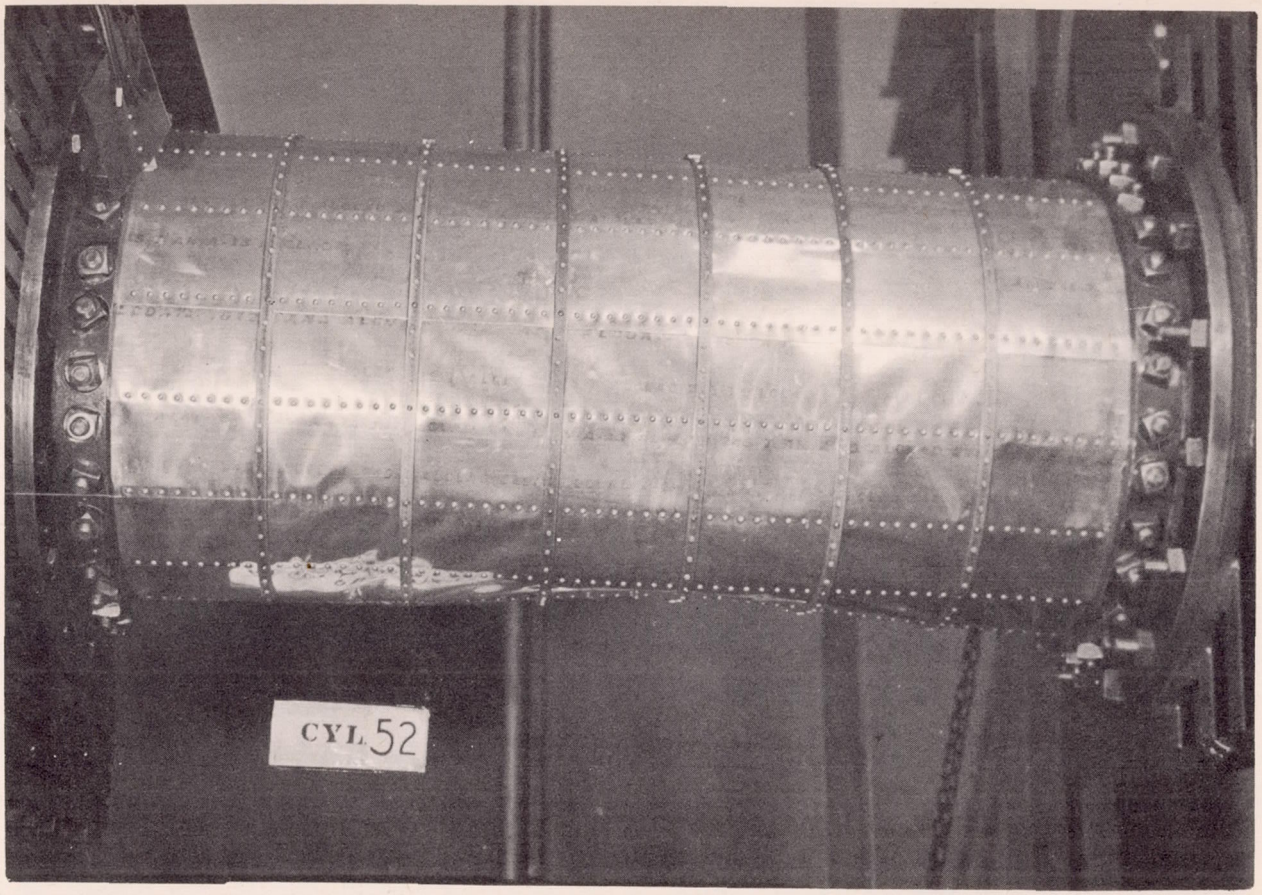

Figure 31.- Photograph of cylinder 52 after buckling.

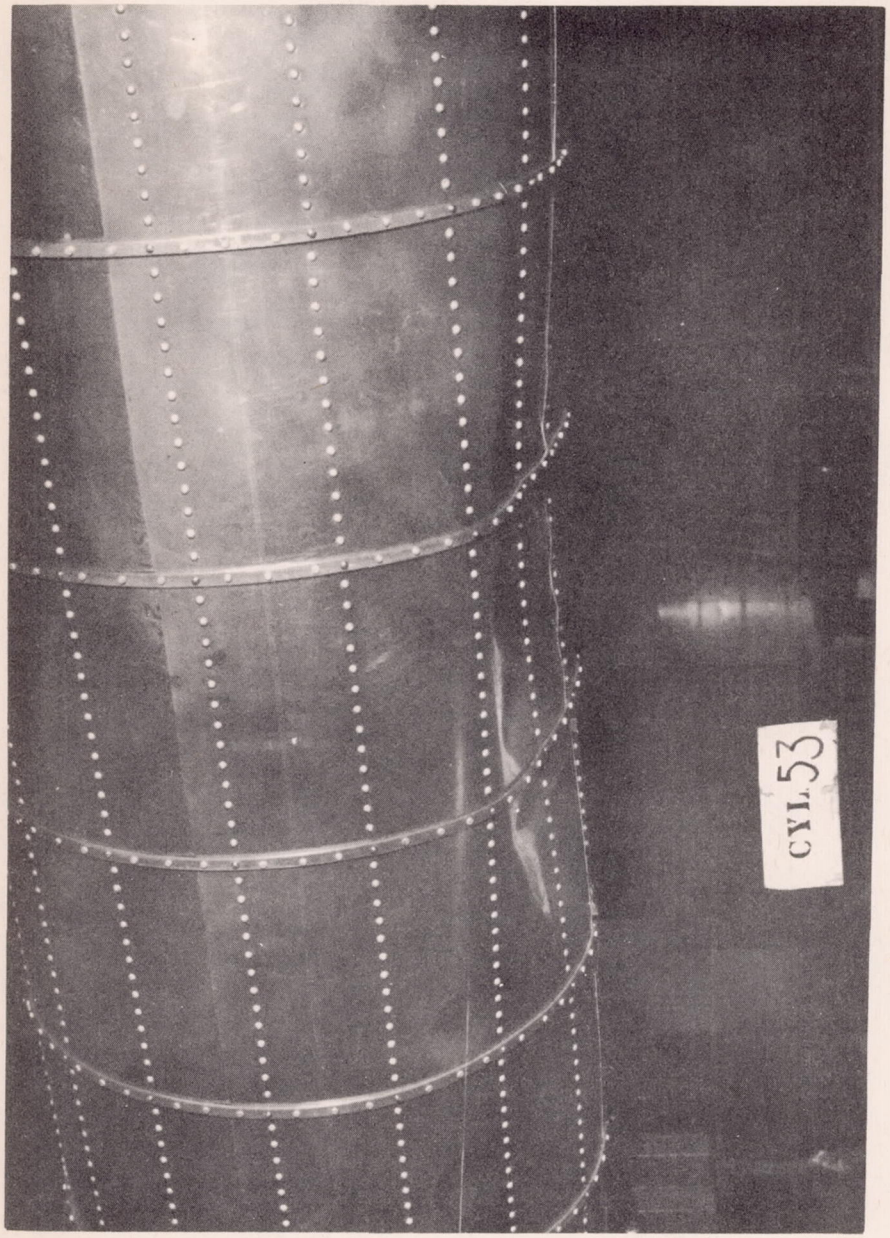

Figure 32.- Photograph of cylinder 53 after buckling.

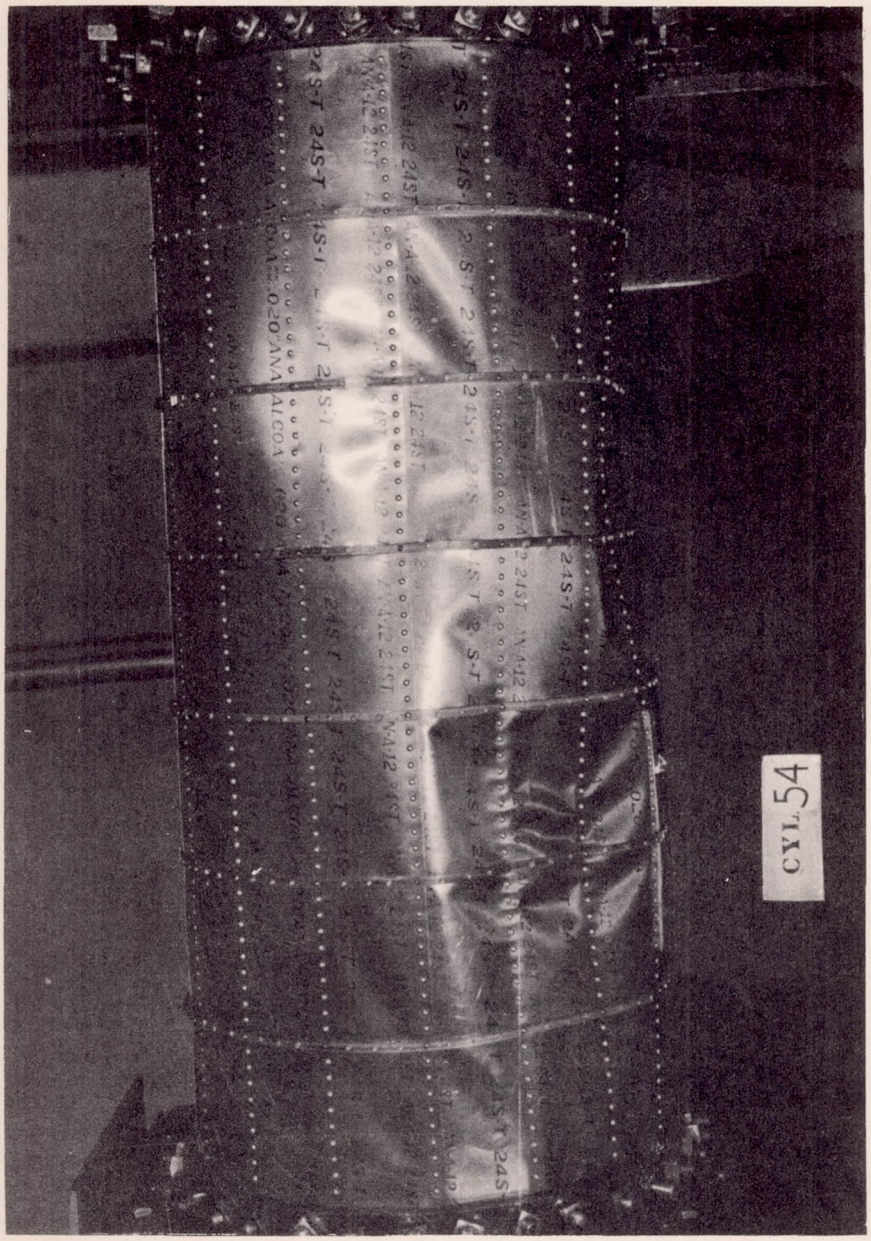

Figure 33.- Photograph of cylinder 54 after buckling.

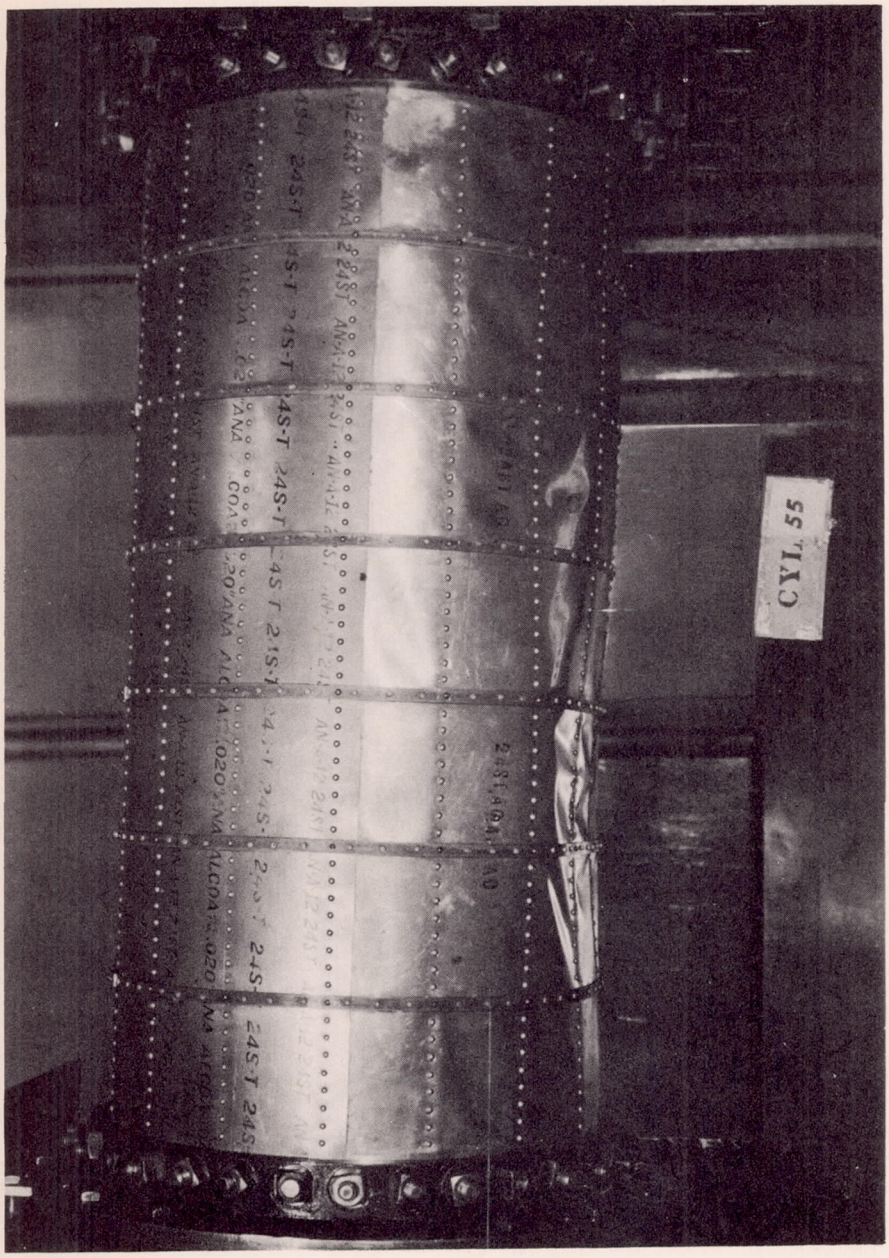

Figure 34.- Photograph of cylinder 55 after buckling.

Figure 35.- Photograph of cylinder 56 after buckling.

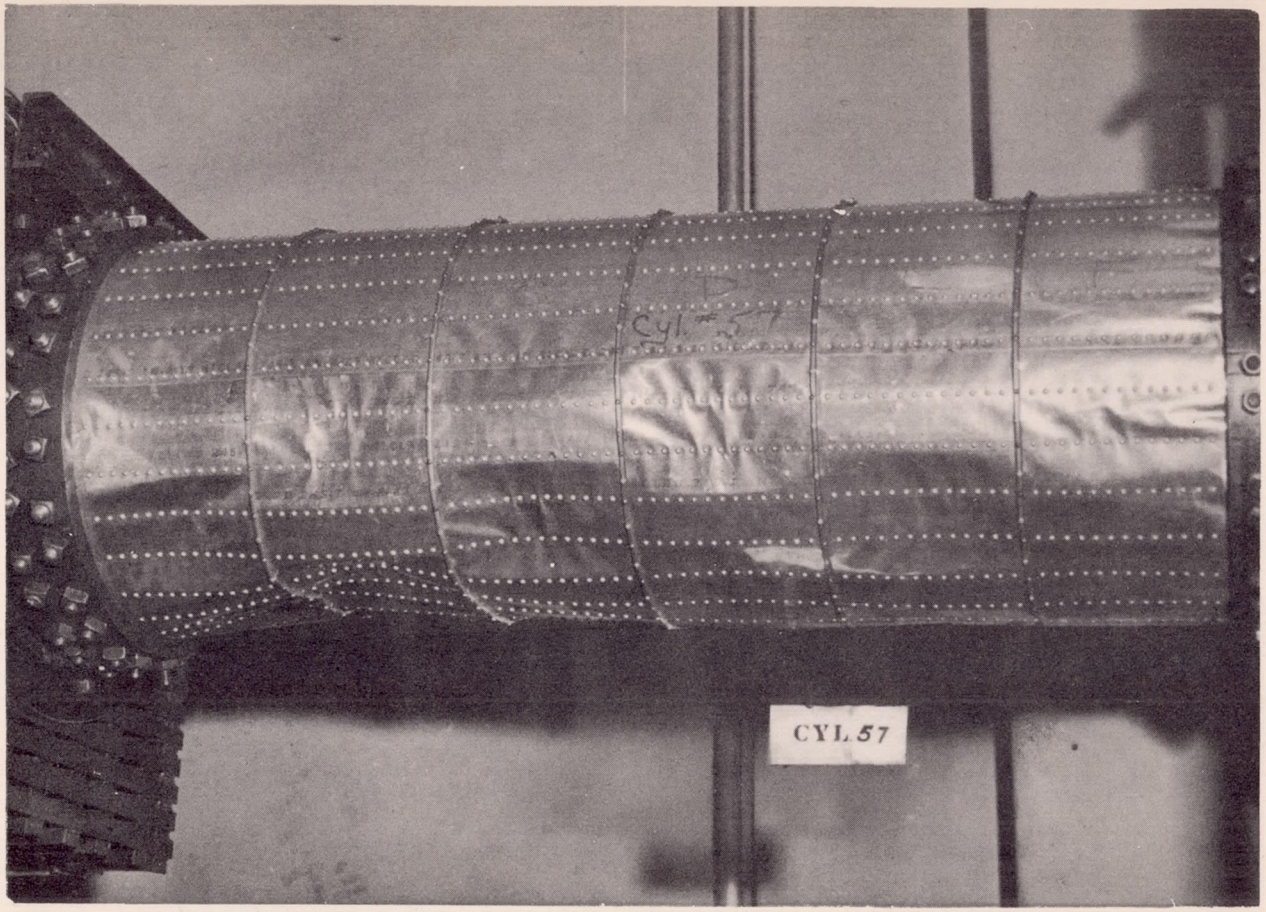

Figure 36.- Photograph of cylinder 57 after buckling.

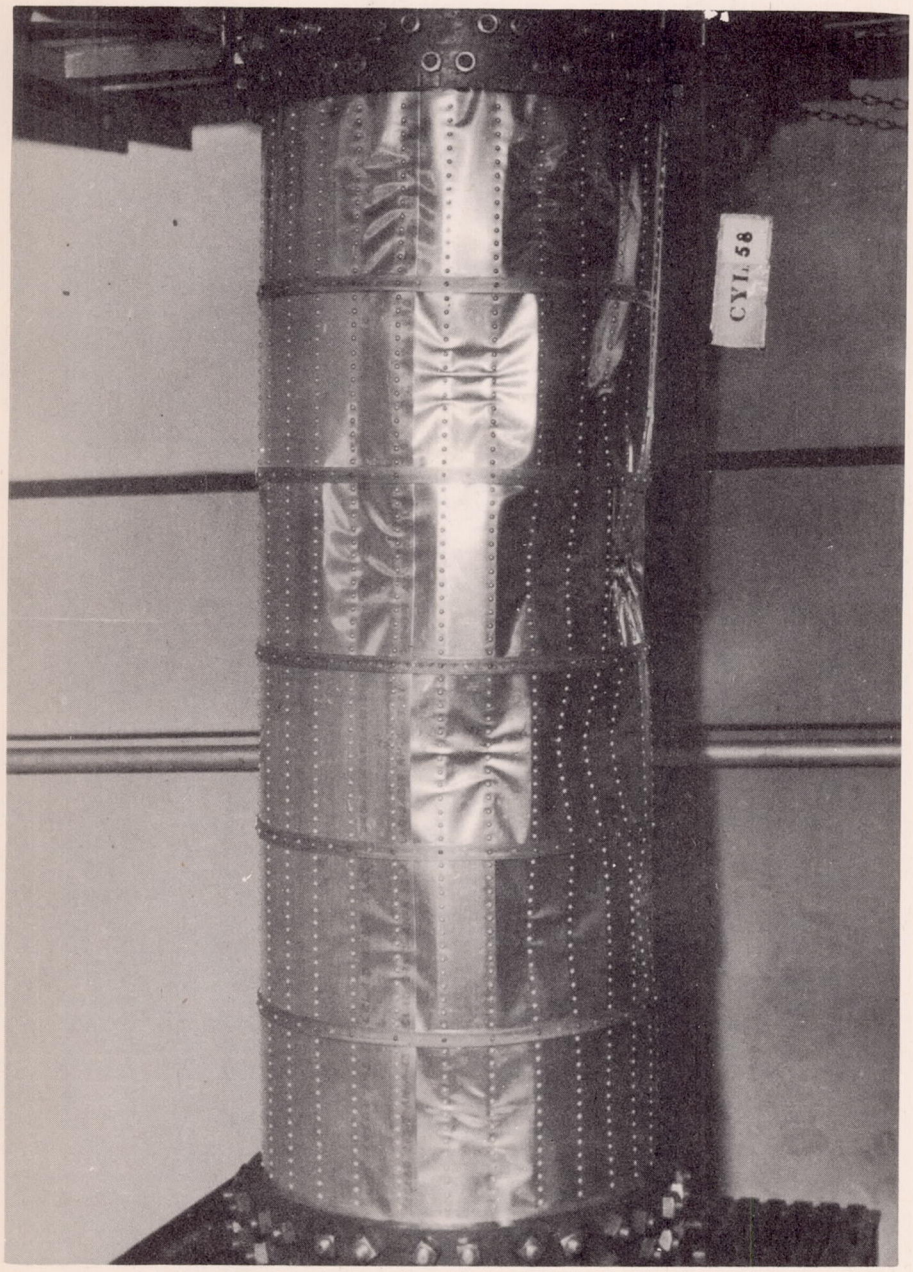

Figure 37.- Photograph of cylinder 58 after buckling.

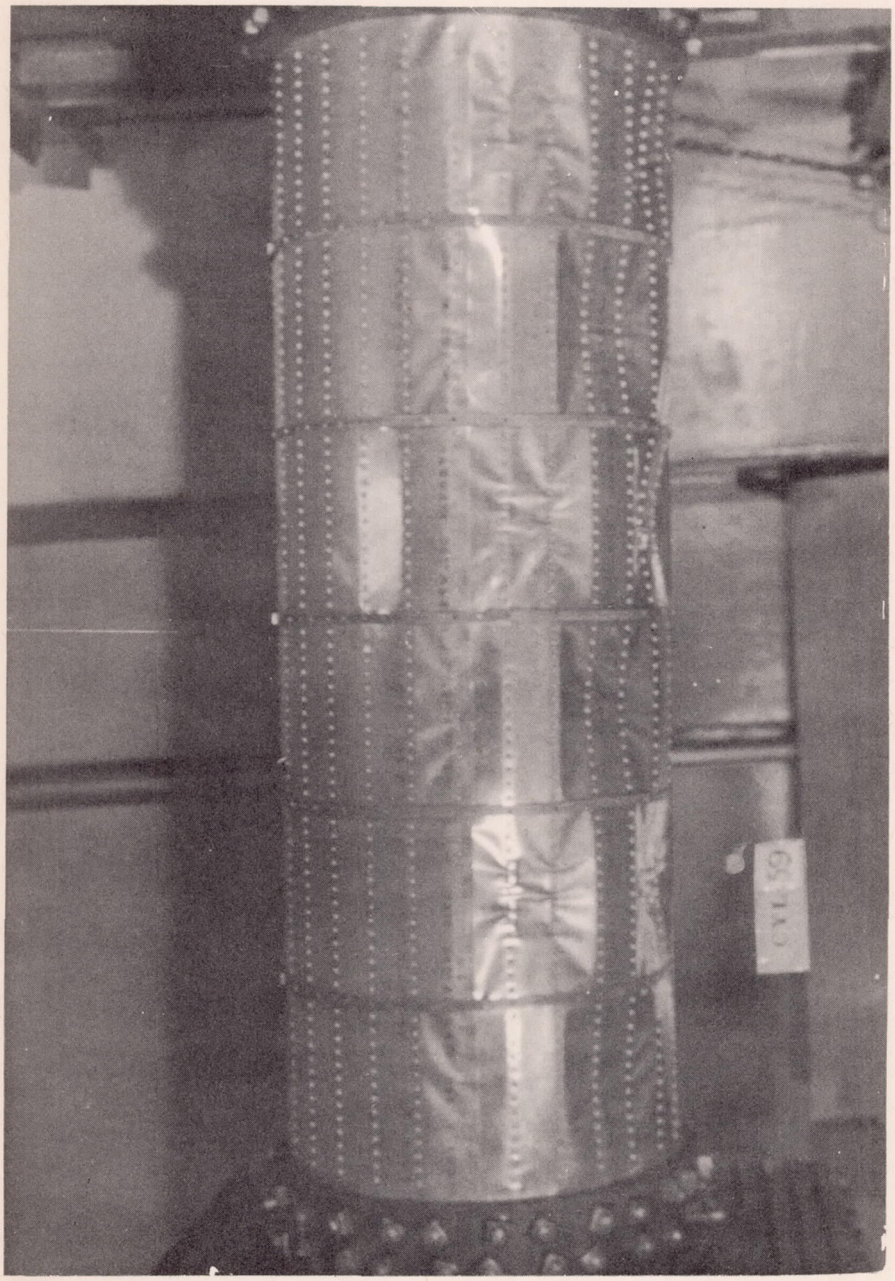

Figure 38.- Photograph of cylinder 59 after buckling.

Figure 39.- Photograph of cylinder 60 after buckling.

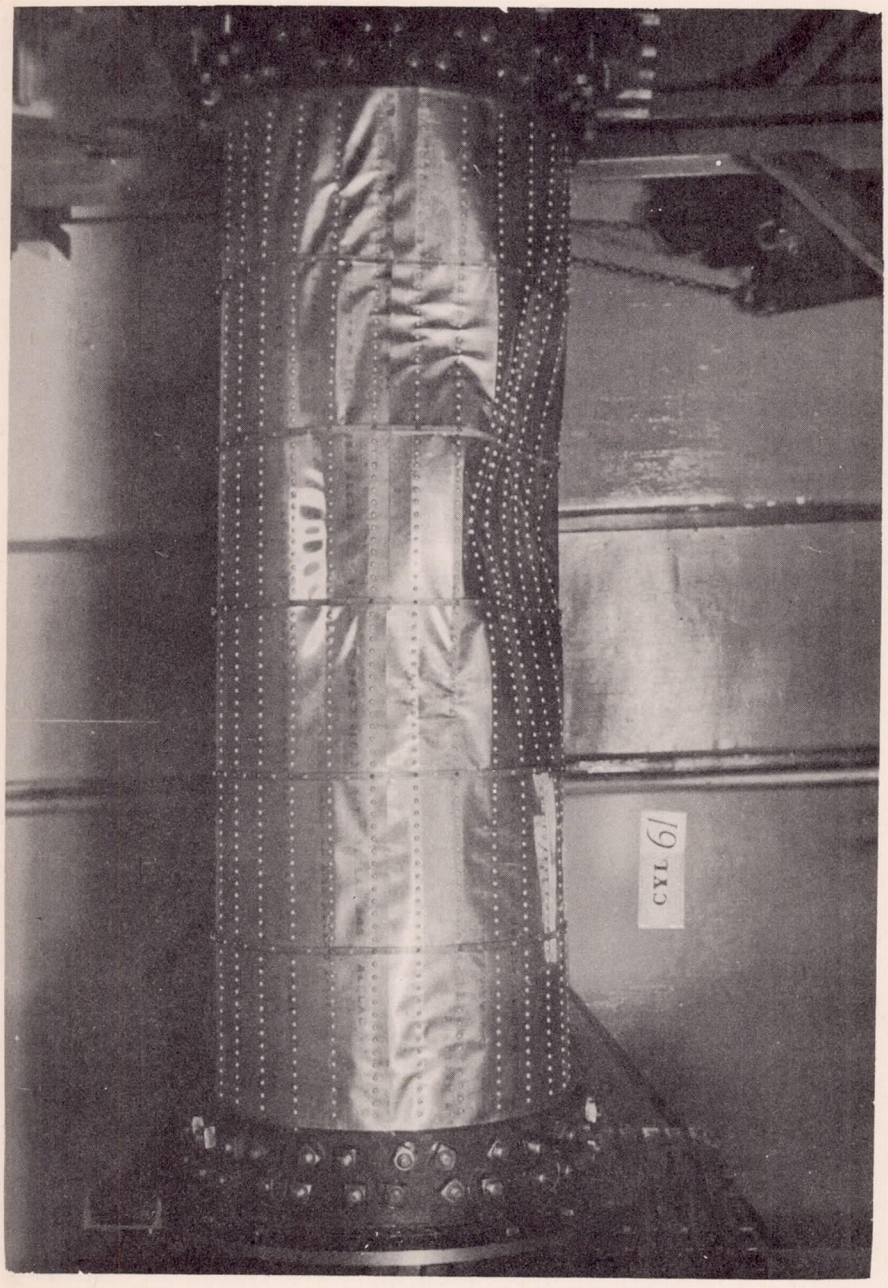

Figure 40.- Photograph of cylinder 61 after buckling.